The effect of bioactive glass particle size and liquid phase on the physical-chemical and mechanical properties of carbonated apatite cement

H. Mabroum, H. Noukrati, H. Ben Youcef, H. Oudadesse, A. Barroug

The Effect of Bioactive Glass Particle Size and Liquid Phase on the Physical-Chemical and Mechanical Properties of Carbonated Apatite Cement

Hanaa Mabroum [a], Hassan Noukrati*[b], Hicham Ben youcef [c], Hassane Oudadesse [d], Allal Barroug*[a,b]

[a] *Cadi Ayyad University, Faculty of Sciences Semlalia, SCIMATOP, Marrakech, Morocco*

[b] *High Institute of Biological and Paramedical Sciences, ISSB-P, Mohammed VI Polytechnic University (UM6P), Morocco*

[c] *High Throughput Multidisciplinary Research Laboratory (HTMR), Mohammed VI Polytechnic University (UM6P), HTMR, Morocco,*

[d] *Univ Rennes, CNRS, ISCR-UMR 6226, F-35000 Rennes, France*

*Corresponding authors:

E-mail**:** hassan.noukrati@um6p.ma (Hassan NOUKRATI)

E-mail**:** a.barroug@uca.ac.ma (Allal BARROUG)

Abstract

This study reports for the first time the effect of particle size of bioactive glass 46S6 on the physico-chemical and mechanical properties of carbonated apatite cement (CPC) composed of brushite ($CaHPO_4$. H_2O) and vaterite ($CaCO_3$). Three particle size ranges were investigated: coarse (BGc: 100-200μm), medium (BGm: 40-100μm), and fine (BGf<40 μm). For the composite formulations, three liquid phases were used: distilled water as a simple setting solution, sodium alginate hydrogel as a cohesion and injectability enhancer, and sodium alginate solubilized in a setting accelerator (Na_2HPO_4) solution (Alg-NaP) to control the setting time.

The changes in the bioglass particle size and the liquid phase lead to clear modifications in the setting, rheological, and mechanical properties of the prepared cements.

The optimization of the different parameters reveals that the formulation with BGc and Alg-NaP as a liquid phase provides the best properties: good injectability of 95%, excellent cohesion, a setting time of 10 minutes that meets the range required by clinicians, and mechanical strength of 10.5 MPa comparable to that of cancellous bone.

Keywords: Calcium phosphate cement, Bioactive glass, Particle size, Physicochemical properties, compressive strength.

1. Introduction

Calcium phosphate cements (CPC) are extensively studied owing to their excellent biocompatibility, osteoconductivity, and their similarity to bone mineral. They were discovered in the 1980s by Brown and Chow [1] and LeGeros et al., [2] as minimally invasive biomaterials for bone repair and regeneration. CPCs are classified according to the final product of the setting reaction, which could be either brushite or apatite [3]. Recently, several studies have focused on improving the mechanical and rheological properties of CPC bone cements by adding either (i) inorganic compounds such as calcium carbonates [4,5] calcium sulfates [7], and bioactive glasses [8–10] or (ii) organic compounds such as biopolymers [12]. To achieve clinical criteria for orthopedic applications, the key properties (i.e., physicochemical, structural, microstructural, cohesiveness, injectability, setting features, mechanical properties) of the paste and hardened cement must be carefully examined while designing the CPC. The control of these characteristics is impacted by several factors, including solubility, pH, particle size, nature of liquid phase, and the liquid to powder ratio (L/P). Several studies investigated the effect of particle size of the initial calcium phosphate powders on CPC properties. Ginebra et al., investigated the effect of powder phase particle size on the micro and nanostructure of α-TCP (85%) and β-TCP (15%) based cement [13]. Thus, decreasing powder particle size induced an increase in the specific surface area of the cement, which strongly accelerated the hydrolysis of α-TCP to calcium deficient hydroxyapatite. Furthermore, the reduction in particle size induced a significant decrease in setting time and expedited the hardening of the cement. However, the fine cement's final saturation compressive strength was only marginally higher than the coarse cement's [14]. Another study investigated the effect of particle size on the curing and handling of a premixed calcium phosphate cement composed of monocalcium phosphate hydrate (MCPH) and β-tricalcium phosphate (β-TCP) [15]. The obtained cements with small particle sizes have higher injection and compressive strength. There was no discernible trend in terms of setting time. Furthermore, the addition of β-TCP granules resulted in cements that were easier to

inject, but the setting time and the strength were negatively affected [15]. Further research has been conducted to improve the properties of CPCs, specifically the addition of bioactive glasses. Bioactive silicate glass has been mixed with CPCs to overcome their clinical limitations, namely their poor injectability and mechanical strength [16].

It was found that adding 45S5 bioglass to the matrix of calcium tetraphosphate (TTCP) and Dicalcium phosphate anhydrous (DCPA)-based CPCs improved injectability and mechanical strength while delaying setting time [10]. El-Fiqi et al., investigated the integration of mesoporous bioactive glass nanoparticles (mBGn) into tricalcium phosphate (α-TCP) and calcium carbonate ($CaCO_3$) based CPCs [17]. The addition of mBGn to cements increased the specific surface area while also hastening the setting reaction of CPCs. The compressive strength of mBGn-containing cements rose the following immersion in SBF, although the injectability of CPCs was greatly improved with the addition of mBGn, in contrast to CPCs.

In another approach, the association of polymers with cements (CPC) has attracted much attention due to the beneficial properties that polymers can bring to cement matrices by improving their rheological, mechanical, and biological properties. Among the most used polymers in the orthopedic field and that have successfully associated cements are chitosan [18], gelatin [19,20], cellulose and its derivatives [21], and alginate [22]. Alginate is the most abundant marine biopolymer and natural polysaccharide that has been widely used in the biomedical field (e.g., tissue engineering, drug delivery, cell therapy) (Lee & Mooney, 2012). Sodium alginate has been incorporated into CaP cement as an additive to improve its rheological and mechanical properties [22,24]. It has been used as a biomaterial for bone repair in combination with other mineral matrices, especially calcium phosphates [25,26] and bioactive glasses [27]. The investigation of the CPC-alginate system demonstrated that the mechanical strength and the cohesion of the cement increased rapidly with the addition of sodium alginate up to 0.8% [28]; although, when the amount of sodium alginate introduced into CPC was greater than 1%wt, the setting has not occurred [28]. Sprio et al. reported that the combination of strontium-substituted hydroxyapatite (Sr-HA) cement with sodium

alginate improved the injectability, cohesion, and mechanical strength of the cement [24]. In recent work, we showed that combining bioactive glass 46S6 (BG) and sodium alginate (Alg) with DCPD-$CaCO_3$ based cement led to the development of composite cement (CPC-BG-Alg) with enhanced injectability, cohesion, and compressive strength [8]. The setting reaction and setting time were accelerated by the addition of BG alone; however, these parameters were delayed when sodium alginate was added to the CPC-BG composite.

Despite numerous studies reported on the association of CPC and BG [10,30,31], the effect of the bioactive glass particle size on the kinetics of the setting reaction, setting time, injectability, cohesion, and compressive strength have not been harnessed. Thus, the current study investigates for the first time the effect of particle size of bioactive glass 46S6 on the setting, injectability, cohesiveness, and compressive strength of CPC based on dicalcium phosphate dihydrate (DCPD) and vaterite ($CaCO_3$). The examined formulations were prepared based on different liquid phases, namely distilled water, alginate hydrogel (Alg), and alginate hydrogel prepared in a sodium phosphate solution (Alg-NaP). The aim was, therefore, to optimize the parameters that result in the best compromise between the properties, allowing for the clinical application of calcium phosphate cement.

2. Materials & Methods

2.1. Materials

2.1.1. Synthesis of DCPD, $CaCO_3$, and Bioactive Glass 46S6

The brushite (Dicalcium phosphate dihydrate, DCPD), vaterite ($CaCO_3$), and 46S6 bioactive glass (BG) were used as solid phases in the cement formulations.

The brushite (DCPD) and vaterite ($CaCO_3$) were synthesized by the double decomposition method as described elsewhere [4,32]. The obtained precipitates were filtered, washed with deionized water, freeze-dried for 72h, and freeze stored.

The 46S6 bioactive glass (BG) was prepared by the melting process as described previously [33]. The inorganic reactants ($CaSiO_3$, $Na_3P_3O_9$, and Na_2SiO_3) were mixed using a mechanical mixer for 20 min. The homogeneous mixture was melted in a Platinum crucible and poured into a preheated die at 500°C near the glass transition temperature. After cooling down to room temperature, the resulting bioactive glass was ground in a mechanical agate mortar and fractionated by vibration sieving to obtain the following particle sizes: the fine particle size (BGf) in the domain < 40 µm, the medium particle size (BGm) in the range of 40-100 µm and the coarse particles between 100 and 200 µm (BGc).

2.1.2. Cements and composites formulation

The powder phase used to formulate the materials was investigated in our previous study and was composed of DCPD, $CaCO_3$, and 46S6 bioactive glass (BG) as reactive powders [8]. CPC-BG cement was obtained by adding 46S6 bioactive glass powders (25% by weight) to the mixture of DCPD and $CaCO_3$. The pastes were then obtained by mixing reactive powders with distilled water as a liquid phase at an L/P ratio of 0.7. For the composite cements two Alginate hydrogel solutions were used, the first consisting of solubilizing the Alginate salts (5 wt%) in distilled water (Alg), and the second (Alg-NaP) was obtained by solubilizing sodium alginate (5 wt%) in a solution of Na_2HPO_4 (NaP, 0.25M). CPC-BG-Alg and CPC-BG-Alg-NaP composites were formulated by mixing reactive powders (DCPD + $CaCO_3$ + 46S6 bioactive glass) with Alg and Alg-NaP hydrogels, respectively.

The pastes of composite cements derived from the powders were placed immediately after preparation in a polyethylene tube at 37°C and 100% relative humidity environment and allowed to set for 48 hours. After maturation for 2 days and drying for 5 days at 37 °C, the hardened and dried cements were characterized.

Table 1 gives an overview of the different prepared composite cements.

Table 1. Various formulations of the composite cements

Samples	**Solid phase**				**Liquid phase**	**L/P**
	$CaCO_3$ (wt %)	**DCPD (wt %)**	**BG**			
			wt %	**particle size (µm)**		
CPC-BGf	37.5	37.5	25	≤ 40	Distilled Water	0.7
CPC-BGm				40-100		
CPC-BGc*				100-200		
CPC-BGf-Alg				≤ 40	5 wt % Alg in H_2O	
CPC-BGm-Alg				40-100		
CPC-BGc-Alg*				100-200		
CPC-BGf-Alg-NaP				≤ 40	5 wt % Alg in Na_2HPO_4 (0.25 M)	
CPC-BGm-Alg-NaP				40-100		
CPC-BGc-Alg-NaP				100-200		

* Formulations used as reference cements from our previous work [8]

2.2. Methods

2.2.1. Physicochemical Characterization

The prepared powders were analyzed by X-ray diffraction (XRD) using Rikagu D/Max-IIIB diffractometer with CuKα source at room temperature. Data were collected between 10 and 70° (2θ) with a precision of 0.02° by steps and a scan speed of $2°min^{-1}$. The chemical composition of the prepared materials was analyzed by transmission Fourier Transform Infrared spectroscopy (FTIR). The acquisition of IR spectra was performed on a Nicolet 5700 spectrometer at room temperature on powdered samples which were embedded in KBr pellets. The spectra were recorded in the range of 4000 cm^{-1} to 400 cm^{-1} with a resolution of 2 cm^{-1}.

Scanning Electron Microscopy (SEM) measurement was performed to evaluate the microstructure of the formulated cements, using TESCAN VEGA3 coupled with an energy dispersive spectrometer (CarbonA). All the specimens were coated with a thin conductive layer of carbon for 30s using a carbonA coater, and the morphologies were observed.

The particle size of the bioactive glass 46S6 powder was determined by a MALVERN MATERSIZER 2000 wet dispersion granulometer.

2.2.2. Setting properties

The effect of particle size of BG on the setting properties of prepared materials was evaluated by examining the setting reaction kinetics and setting time. The setting reaction kinetics were performed to investigate the effect of particle size of BG and the liquid phase nature on the apatite formation in the prepared composites. The prepared cement pastes were incubated for various times (2, 4, 6, and 48 hours) in 100% relative humidity conditions at 37 C°, then freeze-dried to stop the setting reaction of the cements. To compare the setting reaction kinetics of prepared materials, the freeze-dried samples were analyzed by FTIR spectroscopy and XRD analysis. An intensity ratio of apatite/vaterite (I_A/I_V) was also calculated as an indicator of apatite formation. The terms I_A and I_V correspond to XRD peak intensities at 26° and 25.2° (2θ degree) of the newly formed apatite and the residual vaterite, respectively.

Due to the direct impact of BG and its particle sizes on the apatite kinetic formation, the dissolution test of BG was carried out to determine the amount of Ca and Si ions released after two hours of immersion in distilled water and alginate hydrogel. For this purpose, 100 mg of each bioactive glass (BGc, BGm, and BGf) was soaked in 3 ml of distilled water (DW) and alginate hydrogel (5 wt%) for 2 hours and, centrifuged at 4000 rpm for 10 minutes. The amount of Ca and Si released in the solution was determined by ICP-OES using an Optima 7000 DV spectrometer (PerkinElmer).

The setting time was measured according to the ASTM C266-89 standard using a Gillmore testing apparatus. The initial and final setting times of the specimens were determined.

2.2.3. Cohesion and Injectability testing

The rheological properties of prepared materials were investigated in this work in terms of cohesion and injectability. To assess the cohesion, the cements paste, with or without Alg, was injected immediately after preparation (<3 min) into phosphate buffer solution (PBS) and the cohesion was examined visually after 5 min and 24 hours of emersion. The injectability was evaluated by extruding a quantity of 2.0 g of as-prepared paste through a 5 mL disposable syringe, with an opening nozzle of a 2.0 mm diameter while applying a constant force of 12N. The injectability values (I %) were calculated according to the following Equation:

$$I\ (\%) = \frac{wt(injected)}{wt(initial)} * 100 \qquad (1)$$

where I is the injectability, $wt_{injected,}$ and $wt_{initial}$ are the weight of the paste injected through the syringe and the paste initially contained in the syringe. All values were the average of three tests performed for each composite.

2.2.4. Compressive strength

The compressive strength was determined using the Instron 3369 Universal Testing Machine (crosshead speed of 1 mm min^{-1}). The cylindrical Specimens were prepared by mixing the powders and liquid phase, and the resulting pastes were placed in a cylindrical silicone mold (8 mm x 16 mm: diameter x depth), maturated for 2 days in a humid environment at 37°C, and then dried for 5 days at 37°C. All values presented in this work are an average of three samples.

3. Results & Discussion

3.1. Physicochemical Characterization of the prepared materials

3.1.1. Characterization of bioactive glass 46S6 powders

Figure1. illustrates the FTIR spectra in the range between 400 and 1600 cm^{-1} (figure 1.a) and XRD diffractograms (figure 1.b) of the prepared bioactive glasses 46S6 with three particle size ranges, coarse (BGc: 100-200 μm), medium (BGm: 40-100 μm), and fine (BGf < 40 μm). The FTIR results showed that the spectra of prepared bioactive glass powders (BG) are

similar, and the main peaks are attributed to the SiO bond. The absorption bands at approximately 1160 and 450 cm^{-1} are assigned to silicon-oxygen bond [8,34]. In the range between 4000 and 1600 cm^{-1} no band was detected. The XRD diffractograms of BGc, BGm, and BGf are illustrated in figure 1.b and attested that the three patterns are similar presenting a halo between 25° and 35° (2θ degree) attributed to the amorphous structure. Figure 1.d, 1.e, and 1.f depicts the SEM images of BGc, BGm, and BGf, respectively showing a block-like shape morphology for the different particle size ranges.

The particle size distribution of the 46S6 bioactive glass powders, coarse (c), medium (m), and fine (f), obtained by laser is presented in figure 1.c along with the main parameters that characterize the particle size distribution (Table 2).

The particle size distribution of the synthesized bioactive glass powders, coarse (BGc), medium (BGm), and fine (BGf), was determined by laser diffraction (figure 1.c). The distribution is monomodal for all prepared glasses, and the median particle size for BGf, BGm, and BGc is 20 ± 1 μm, 81 ± 3 μm, and 198 ± 8 μm, respectively. Table 2 summarizes the particle-size distribution parameters attesting that for BGf, 10% of particles by volume were smaller than 15 ± 1 μm, 50% were smaller than 20 ± 1 μm, and 90% were smaller than 47 ± 2 μm.

For the BGm, 10% of particles by volume were smaller than 48 ± 2 μm, 50% were smaller than 81 ± 3 μm, and 90% were smaller than 172 ± 7 μm. Also, 10% of particles by volume of the coarser bioactive glass (BGc) were smaller than 131 ± 5 μm, 50% were smaller than 198 ± 8 μm, and 90% were smaller than 295 ± 12 μm.

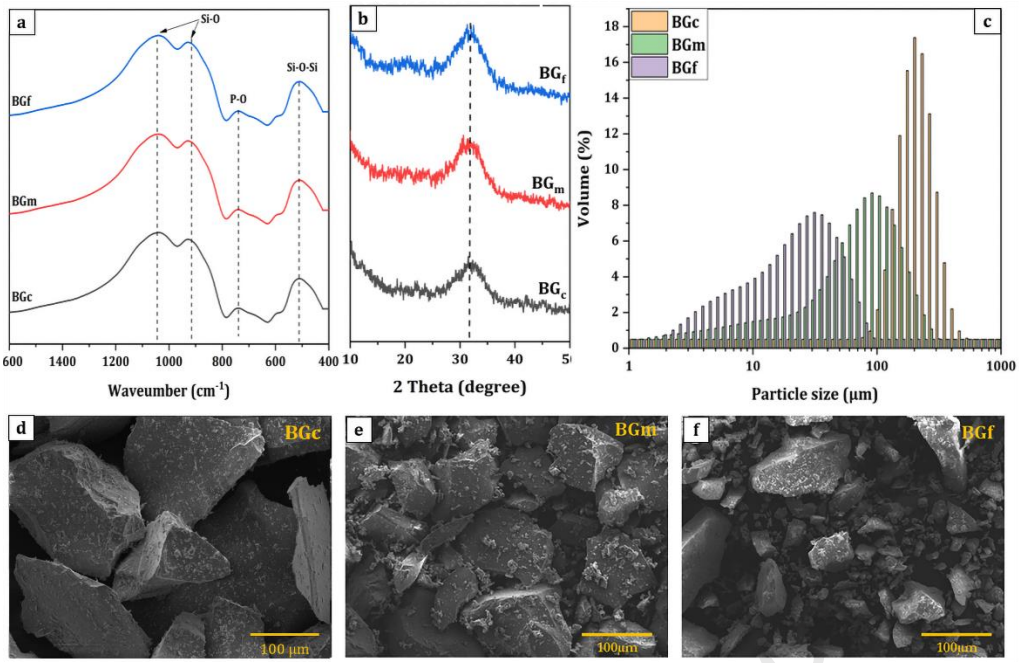

Figure 1. FTIR (a) and XRD (b), particle size distribution (c), and SEM micrographs of BGc (d), BGm (e), and BGf (f) of the bioactive glass 46S6 powder.

Table 2. Particle-size distribution parameters of the BG powders

Bioactive glass	D (10) (µm)	Median Size, D (50) (µm)	D (90) (µm)	Particle size volume average, Mv (µm)
BGc	131 ± 5	198 ± 8	295 ± 12	207 ± 8
BGm	48 ± 2	81 ± 3	172 ± 7	90 ± 4
BGf	15 ± 1	20 ± 1	47 ± 2	23 ± 1

3.1.2. Characterization of hardened composite cement

Figure 2 illustrated XRD patterns (a) and FTIR spectra (b) of hardened cements (CPC and CPC-BGm) compared to reactive powders (DCPD and $CaCO_3$). The XRD analysis revealed a similarity in the diffractograms of the formulated cements showing the presence of two phases: the newly formed apatite particularly at 25.7° and 32.2° and the residual vaterite at 24.8°, 27°, and 32.7° (2 theta degree). However, no DCPD peak was detected in the diffractogram attesting that this reagent was completely consumed during the reaction with vaterite. Furthermore, the addition of glass BGm did not alter the structure of the CPC cement. The effect of BG particle size and the liquid phase on the cements' composition will be examined in the reaction kinetics section.

The FTIR spectra of the CPC and CPC-BGm cements display a similar appearance with a wide and intense band in the domain 3000-3400 cm^{-1} indicating the presence of water adsorbed, as well as the presence of phosphate bands in 1000-1150 cm^{-1} and 550-650 cm^{-1} regions attributed to the newly formed apatite. The spectra were also marked by the existence of residual vaterite in the region of 1400-1500 cm^{-1} characteristic of the vibration ν_3 of carbonate and the band at 876 cm^{-1} typical of the ν_2 vibration of carbonate. In addition, a low-intensity band noticed at 470 cm^{-1} and corresponding to Si-O-Si bending was attributable to the glass BGm incorporated into the formulated cement CPC-BGm.

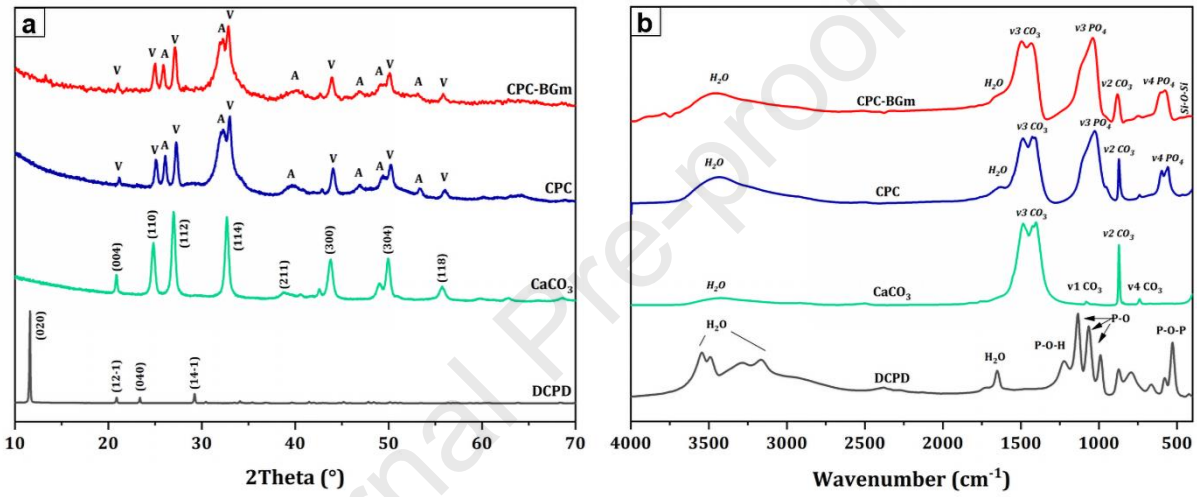

Figure 2. XRD patterns (a) and FTIR spectra (b) of CPC and CPC-BGm compared to the DCPD and $CaCO_3$ phases (A: Apatite, V: Vaterite).

3.1.3. Cements and composites properties

3.1.3.1. Setting reaction

In order to follow the evolution of the composition of the prepared cements over time, during setting and hardening, the reaction was stopped by freeze-drying cement pastes at different maturation times (2, 4, 6, and 48 hours) and analyzed using FTIR and XRD techniques. The setting behavior of the prepared materials was discussed regarding the BG particle size and the nature of the liquid phase.

The evolution of the XRD peaks of brushite and vaterite as reactants and apatite as a newly formed phase in the range of 10 - 40° was used to assess the setting kinetics. Figure 3 depicts the XRD patterns of all formulated as a function of reaction time. The cements CPC-BGf,

CPC-BGm, and CPC-BGc formulated with distilled water (figure 3.a) showed that the typical peaks of vaterite and DCPD are all indexed in the composite's patterns after 2 hours with a decrease in the intensity of the most intense peak of DCPD at 12° by increasing the particle size of BG. Furthermore, the XRD patterns of CPC-BGc and CPC-BGm revealed the appearance of apatite peaks at 25.7° and 32.2, while this phase is not noticeable for the composite CPC-BGf; this observation suggests that the reaction is faster when increasing the BG particle size.

After 4 hours of reaction, the XRD diffractograms of CPC-BGc and CPC-BGm cements appear to be similar, indicating the disappearance of peaks characteristic of the DCPD phase at 12° (2 Theta degree); however, this phase persisted in the pattern of the CPC-BGf cement. Moreover, the presence of typical apatite and vaterite peaks anchored all three diffractograms. These diffractograms became similar after 6 up to 48 hours of reaction, showing the presence of apatite peaks whose intensity varies according to the size of the BG particles. When the BG size is coarse, the intensity of the two apatite peaks (located at 25.7° and 32.2°) was higher than those of cements prepared with BGm and BGf. In addition, vaterite peaks were also indexed which intensity varies inversely to those of apatite.

In the presence of the alginate hydrogel, the trend was reversed compared to distilled water showing that the reaction was accelerated for the CPC-BGf-Alg and CPC-BGm-Alg composites and slowed down for the CPC-BGc-Alg composite (Figure 3.b). The CPC-BGc-Alg composite had a different chemical setting behavior compared to the other two composites. The XRD patterns of CPC-BGf-Alg and CPC-BGm-Alg are nearly identical, indicating that the apatite phase began to form after 2 hours of reaction. DCPD and vaterite peaks were present in all composite patterns, with a decrease in the intensity of DCPD as the BG particle size decreased. Furthermore, the CPC-BGm-Alg and CPC-BGf-Alg diffractograms indexed low-intensity peaks of DCPD with the appearance of apatite peaks located at 25.7° and 32.2°. However, no apatite peaks were identified in the CPC-BGc-Alg pattern. After 4 hours of reaction, the XRD diffractograms of the CPC-BGf-Alg and CPC-

BGm-Alg composites are still similar and showed the total disappearance of the DCPD peaks as well as the presence of peaks characteristic of apatite and vaterite, with an increase of apatite intensity peaks. However, the CPC-BGc-Alg composite showed a different setting behavior than the other two composites, supported by the presence of DCPD peaks as well as low-intensity peaks that appeared and are attributed to the apatite phase. After 6 hours of reaction, the DCPD peaks disappeared in CPC-BGc-Alg, and all composite diffractograms became similar and revealed the presence of typical vaterite and apatite peaks. After 48 hours, the patterns appeared to be similar, and the intensity of the apatite peaks increased, attesting the growth of the apatite phase even after the disappearance of the DCPD phase (limiting reagent), suggesting that the setting reaction is governed by the formation and growth of an apatite layer on the bioactive glass and vaterite surfaces.

When compared to formulations containing alginate hydrogel as a liquid phase, the addition of the setting accelerator in alginate hydrogel solution appears to have a significant effect on the reaction kinetics after 2 hours. Indeed, the XRD diffractograms of CPC-BGf-Alg-NaP and CPC-BGm-Alg-NaP composites indexed all apatite and vaterite peaks, while the DCPD peaks completely disappeared (Figure 3.c). For the same reaction period, the XRD diffractogram of the CPC-BGc-Alg-NaP composite cement revealed the presence of apatite peaks, which were not present in the composite formulated with alginate hydrogel solution alone. The diffractogram also indicated the presence of DCPD and vaterite peaks. After 4 hours, the three XRD patterns for all formulated composites are similar to those obtained with alginate alone, displaying the presence of peaks attributed to apatite and vaterite for CPC-BGm-Alg-NaP and CPC-BGf-Alg-NaP. The diffractogram of the CPC-BGc-Alg-NaP composite revealed that the DCPD phase persisted and indicated the typical peaks of apatite and vaterite. The diffractograms became similar between 6 and 48 hours of maturation, indicating the disappearance of the DCPD peaks, and apatite and vaterite peaks were all indexed. Furthermore, the intensity of the apatite peaks increased when compared to alginate alone

attesting the presence of a second reaction between accelerator and vaterite and leading to the formation of apatite.

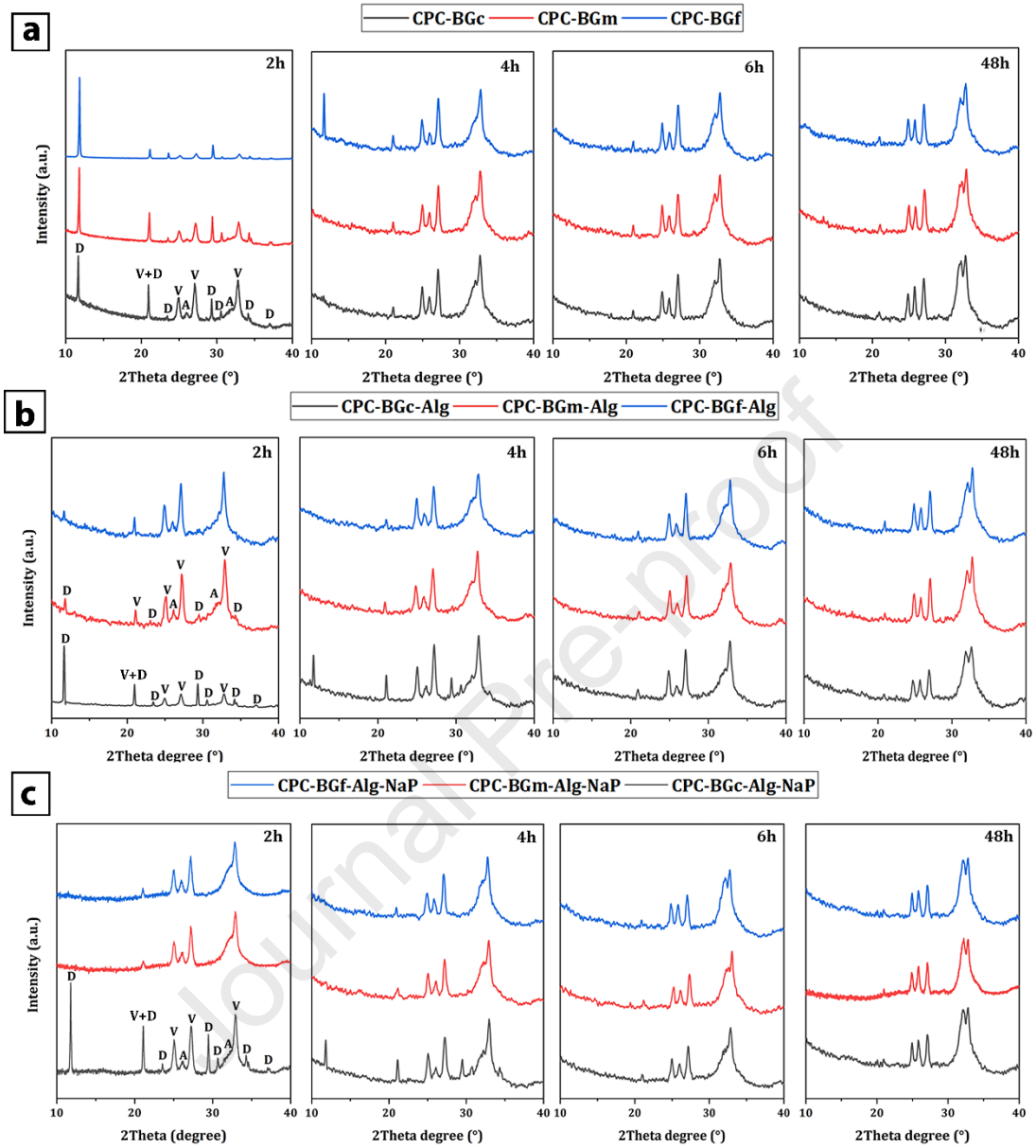

Figure 3. XRD patterns of the formulated materials as a function of reaction time, in distilled water (a), in alginate hydrogel (b), and alginate with NaP (c); (D: DCPD, V: $CaCO_3$ and A: Apatite)

To evaluate the formation of apatite during the setting reaction of the formulated cements, a ratio of the XRD peak intensities of apatite at 25.7° and vaterite at 24.8° was calculated using origin software. Figure 4 showed the variation of the apatite/vaterite intensity ratio (I_A/I_V): as a function of reaction times for all formulated composites. The results of the intensity ratio assessment (I_A/I_V) supported the findings from the XRD analysis, attesting that the setting

reaction could be significantly affected by BG particle size as well as the liquid phase. When distilled water is used as the liquid phase, the cement made with BGc exhibited the highest intensity ratio for all reaction times, followed by CPC-BGm, and CPC-BGf.

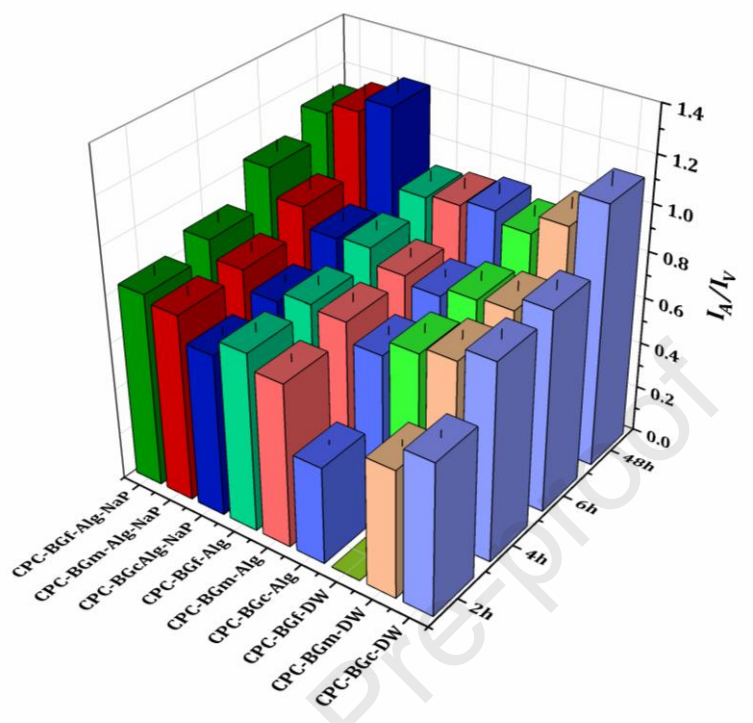

Figure 4. Intensity ratio (I_A/I_V) obtained from the XRD patterns of prepared materials as a function of incubation time.

When alginate hydrogel was used as the liquid phase, this trend was reversed, indicating that the CPC-BGf-Alg composite cement had the highest intensity ratio during the first 6 hours of reaction. After 48 hours of reaction, the intensity ratio for CPC-BGc-Alg composite increased significantly, followed by CPC-BGm-Alg composite and CPC-BGf-Alg with the lowest I_A/I_V. Moreover, the intensity ratio of the prepared composite with Alg seemed to be lower than those formulated with distilled water, and it could be due to the ionic exchange of Na and Ca to form the calcium alginate. Furthermore, in the presence of Alg-NaP as a liquid phase, the same trend was observed compared to Alg hydrogel alone, indicating that during the first hours, CPC-BGf-Alg-NaP has the highest intensity ratio. After 48 hours, the trend appears to be reversed, and the composite (CPC-BGf-Alg-NaP) has the lowest ratio compared to the other two composites (CPC-BGm-Alg-NaP and CPC-BGc-Alg-NaP).

Furthermore, when compared to distilled water and alginate hydrogel, the intensity ratio is the highest in the presence of NaP.

Focusing the comparison on the end of the reaction (48h), the highest intensity ratio (I_A/I_V) was obtained using Alg-NaP as liquid phase, followed by distilled water and alginate gel, respectively. Indeed, the addition of sodium alginate delayed the apatite formation after 48 hours of reaction due to the viscous aspect of the hydrogel, which slows the diffusion of Ca and P ions, thereby inhibiting apatite precipitation. The use of Na_2HPO_4 as a setting liquid solution for the solubilization of Alg salt has significantly promoted the formation of apatite and it could be attributed to a secondary reaction between the phosphate ions of Na_2HPO_4 and the calcium ions of the residual vaterite. This difference in the intensity ratio (I_A/I_V) could be explained by ions supersaturation which is higher in the case of Na_2HPO_4 and lowest for distilled water and alginate hydrogel.

Complementary characterization was performed by FTIR analyses to assess the setting reaction kinetics of the prepared composite cements. The setting kinetics were evaluated through the evolution of FTIR bands of brushite as a limiting reactant and apatite as a newly formed phase. Figure 5 illustrated FTIR spectra of all prepared composites in the range of 450 to 800cm^{-1} after intensity normalization.

The FTIR spectra of the formulated cements using distilled water as a liquid phase after 2 hours of reaction (figures 5.a), are not similar. The FTIR spectrum of CPC-BGf showed the presence of bands attributed to DCPD compound at 790, 670, 577, and 526 cm^{-1} characterizing phosphate groups. These bands are also observed in the CPC-BGm spectrum with the appearance of new bands at 560 and 600 cm^{-1} attributed to the newly formed apatite which are absent in CPC-BGf spectrum. Compared to CPC-BGf and CPC-BGm spectra, the spectrum of CPC-BGc is marked by the presence of a DCPD band at 526 cm^{-1} with low intensity and completely disappeared of the other bands of DCPD. In addition, CPC-BGc revealed the presence of apatite bands at 560 and 600 cm^{-1} attributed to υ4 vibration mode of phosphate groups. After 4 hours of reaction, the FTIR spectra of CPC-BGc and CPC-BGm

are similar and showed the total disappearance of brushite and the presence of bands typical to the reprecipitated apatite at 560 and 604 cm^{-1}. The shoulder in the CPC-BGc spectrum at 525cm^{-1} could be attributed to the Si-O-Si band characteristic of bioactive glass. However, the CPC-BGf spectrum revealed the presence of all DCPD bands with low intensities compared to 2h. The characteristic bands of apatite are not observed as shown in the XRD patterns and this could be due to the overlapping of the DCPD and apatite bands in this domain. From 6 hours to 48 hours of reaction, the FTIR spectra of the cements become similar and are marked by the presence of apatite (560 and 604 cm^{-1}) and vaterite (at 750 cm^{-1}) bands and the absence of all DCPD bands attesting to the total consumption of this reagent.

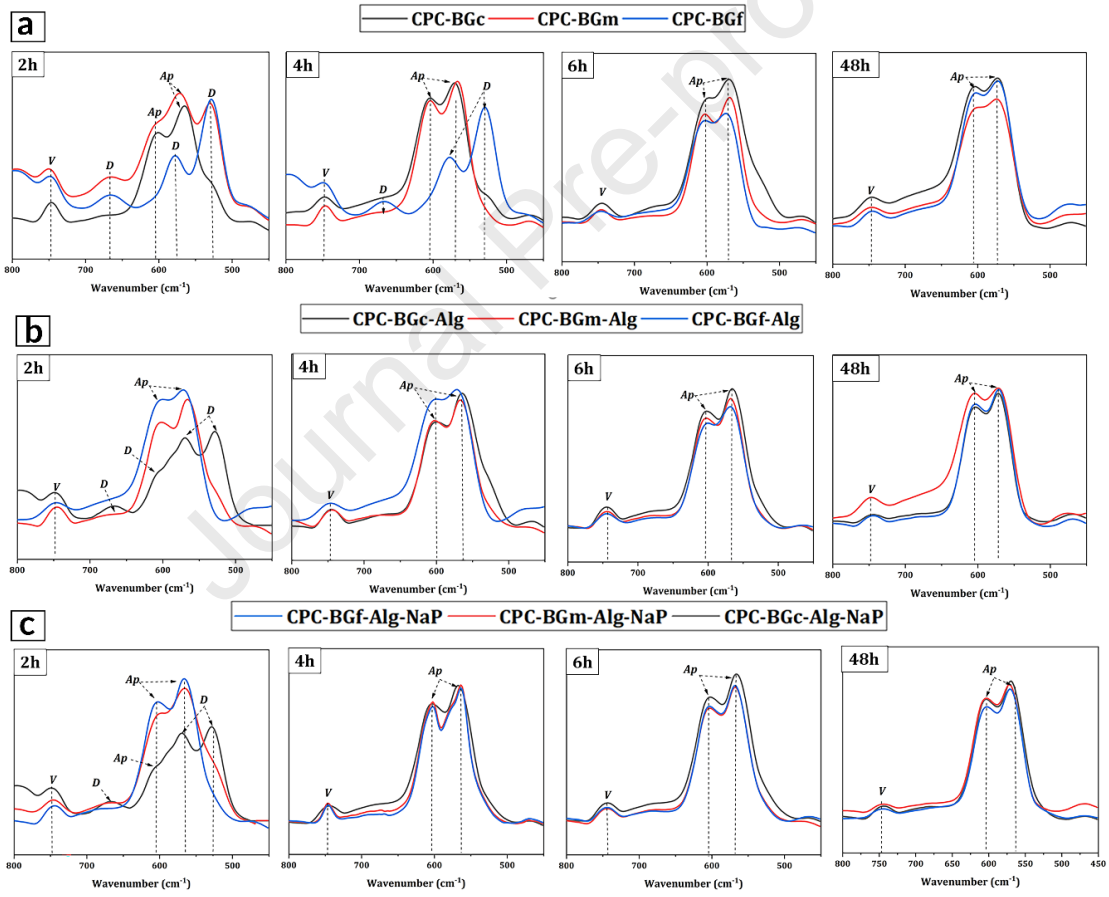

Figure 5. FTIR spectra of formulated materials in distilled water (a), alginate hydrogel (b), and Alg-NaP gel (c).

The assessment of the setting reaction of cements prepared with distilled water as a liquid phase showed that during the first hours of reaction, the CPC-BGc cement exhibited the fast-setting reaction resulting in the rapid apatite formation. Figure 5.b depicted the chemical

setting behavior of the cement formulated in the presence of sodium alginate hydrogel as a liquid phase. The results revealed that after 2 hours of reaction, the CPC-BGc-Alg composite spectrum is marked by the presence of all DCPD bands (at 790, 670, 577, and 526 cm^{-1}) and the appearance of low-intensity band attributed to the reprecipitated apatite at 604 cm^{-1}. The vaterite band was also identified in the spectrum at 750 cm^{-1} with low intensity. Besides, CPC-BGm-Alg and CPC-BGf-Alg possessed similar FTIR spectra, attesting the complete absence of DCPD bands and the presence of bands typical to the newly formed apatite and the residual vaterite. After 6 hours of reaction, the FTIR spectra of the three composites showed a similar chemical setting behavior, revealing the presence of the characteristic bands of apatite between 550 and 650 cm^{-1}.

The use of alginate hydrogel as a liquid phase for the formulation of composite cements revealed that the setting reaction was slowed down for the composite formulated with a coarse bioactive glass (CPC-BGc-Alg), while the reaction was accelerated by the addition of this polymer for the composites CPC-BGm-Alg and CPC-BGf-Alg, attesting to an inverse effect when using distilled water as a liquid phase. The setting behavior was evaluated when sodium alginate solubilized in Na_2HPO_4 (NaP) was used as the liquid solution (Figure 5.c). The obtained results showed that in the presence of the NaP component, the composites' setting reaction was not affected compared to the composites formulated with the hydrogel alone. After 2 hours of reaction, the FTIR spectrum of the CPC-BGc-Alg-NaP composite revealed the presence of all the characteristic DCPD bands (at 790, 670, 577, and 526 cm^{-1}) whose intensity decreased for the CPC-BGm-Alg-NaP and completely disappeared in the spectrum of the composite CPC-BGf-Alg-NaP. The two apatite bands are also present in the FTIR spectrum of CPC-BGm-Alg-NaP, whereas the FTIR spectrum of the composite with a coarse bioactive glass (CPC-BGc-Alg-NaP) had only one apatite band at 560 cm^{-1}. Furthermore, the typical band of residual vaterite at 750 cm^{-1} is present in all three FTIR spectra. Beyond 4 hours of reaction, the FTIR spectra were similar, showing the presence of bands that characterize apatite and vaterite.

The XRD and FTIR analyzes are in agreement and have revealed that the particle size of bioactive glass and liquid phase affected the setting reaction kinetics and consequently the apatite formation. Three mechanisms could govern the setting reaction kinetics of brushite, vaterite, and bioactive glass 46S6 types of cement. The first mechanism is based on an acid-base reaction between DCPD and $CaCO_3$, which resulted in the formation of carbonate apatite [35], as illustrated in the reaction below:

$$4\ CaCO_3 + 6\ CaHPO_4.2H_2O \rightarrow Ca_{10-x-y}(PO_4)_{6-x-y}(HPO_4)_x(CO_3)_y(OH)_{2-x-y} \quad (1)$$

$$\text{Avec } 0 < x + y < 2$$

The second mechanism could be related to a chemical interaction between calcium and phosphate ions derived from the dissolution of bioactive glass and brushite phases, resulting in a second setting reaction and leading to the reprecipitation of the apatite phase. Furthermore, it is well known that when the silicate-based bioactive glass comes into contact with an aqueous medium, it forms a calcium phosphate layer on its surface [36,37]. Therefore, the formation of the apatite layer on the bioactive glass 46S6 surface could be the third mechanism that may influence the setting reaction kinetics [38]. These competing chemical mechanisms govern the setting reaction of the cements during the first hours.

Several factors could influence the setting properties of bone cements, including the liquid/powder ratio, the nature of the liquid phase, the particle size of the initial products, the solubility of the precursors, the pH...etc [39]. This study evaluated the effect of particle size of bioactive glass 46S6 and the nature of the liquid phase on the kinetics of cement setting reaction.

According to the XRD and FTIR results, these two factors influenced the setting reaction, particularly during the first hours. Indeed, the setting reaction was modified based on the size of the BG for the composites prepared in the presence of distilled water, demonstrating that the kinetic was faster for the cement with the coarse bioactive glass (CPC-BGc), followed by the cement CPC-BGm. However, the cement prepared with fine BGf was the least reactive during the first hours. This effect brought by increasing the size of BG promotes the

formation of apatite in the presence of distilled water could be attributed to the lower water absorption rate for BGc which would facilitate the penetration of water between the particles and then the dissolution of the reactants, as opposed to cement formulated with BGf, which absorbed more water. The particle size of the initial reactive powders is known to influence the amount of water absorbed, the smaller the size of the particle is, the higher the absorption of water [40]. The solubility of the raw materials is also a crucial parameter that could impact the dissolution and reprecipitation mechanisms. Indeed, the decrease of BG particle size could improve its solubility and then its dissolution leading to high ions concentration in terms of silicate and calcium, as demonstrated by ICP analysis. Table 3 illustrated the results of the chemical analysis of Ca and Si elements released from the bioactive glasses (BGc, BGm, and BGf) after 2 hours of immersion in distilled water and alginate hydrogel. The results showed that after 2 hours of immersion in distilled water, Ca and Si concentrations in the BGf bioactive glass were found to be high, with values of 2.83 ± 0.170 and 0.81 ± 0.049 mg/l., respectively. The BGm bioactive glass produced a Ca concentration of 1.42 ± 0.080 mg/l and Si concentrations of 0.26 ± 0.016 mg/l. BGc, on the other hand, has the lowest Ca and Si concentrations with about 0.527 mg/l Ca and 0.049 mg/l (table 3), respectively. In the alginate hydrogel, the concentrations of released Ca and Si ions released from bioactive glasses, BGf, BGm, and BGf, are higher than in distilled water. The results obtained attested that the BG particle size did not affect the Ca concentration, and it is around 5.16 ± 0.310 mg/l for BGc, 5.18 ± 0.311 mg/l for BGm, and 5.54 ± 0.330 mg/l for BGf. The highest concentration of Si released in the alginate hydrogel is that of BGf, with a value of 7.457mg/l, followed by BGm (5.913mg/l), and BGc had the lowest concentration of Si, which is around 4.152 mg/l. These results attested that the finer BGf released higher ions amounts than BGm and BGc respectively. Based on these results the delay in the formation of apatite in the case of CPC-BGf and CPC-BGm during the first hours of reaction could be explained by the high concentration of Si known by its inhibitory effect on the formation of apatite. It was reported in the literature that the incorporation of Si into an α-tricalcium phosphate-based cement

delayed the conversion of α-TCP to CDHA and a silica gel deposited to the initially precipitated apatite crystals have limited their growth [41]. A similar effect was attested by Tanizawa and Suzuki who reported an inhibiting effect of the silicate ions on the transformation of dicalcium phosphate dihydrate (DCPD) into apatite [42].

Contrary to the trend observed for formulations with distilled water, the composites prepared in the presence of sodium alginate, showed an acceleration in the setting reaction by decreasing the size of bioactive glass. This effect can be explained on the one hand by the increase in the solubility of BG in the presence of Alg as demonstrated by the ICP analysis. Indeed, the presence of Ca and P ions in high concentrations favors the formation of apatite. On other hand this effect could be explained by the possibility of a complexation reaction between silica and carboxylic acid functional groups on the mannuronic and guluronic acids in alginate [43], resulting in a decrease in the concentration of free Si ions in the medium and thus eliminating its inhibiting effect on the formation of apatite [43].

To confirm this interaction between sodium alginate and Si, the BGc-Alg powders were recovered after immersion for 2 hours in an aqueous sodium alginate solution and dried at 37°C in order to evaluate their composition through FTIR analysis (figure 6). The results of this analysis showed the appearance of new bands located at 1250 cm^{-1} attributed to the vibration of the Si-O-C bond [43] and at 1470 cm^{-1} which could be typical to Si-C band. The appearance of these bands attests to the existence of interactions between alginate and silicon in the bioactive glass.

Table 3. ICP results of solutions containing BGc, BGm, and BGf.

Materials	Ca (mg/L)	Si (mg/L)
BGc-DW	0.05 ± 0.003	0.53 ± 0.03
BGm-DW	0.26 ± 0.02	1.42 ± 0.08
BGf-DW	0.81 ± 0.05	2.83 ± 0.17
BGc-Alg	5.16 ± 0.31	4.15 ± 0.25
BGm-Alg	5.18 ± 0.31	5.91 ± 0.35
BGf-Alg	5.54 ± 0.33	7.46 ± 0.44

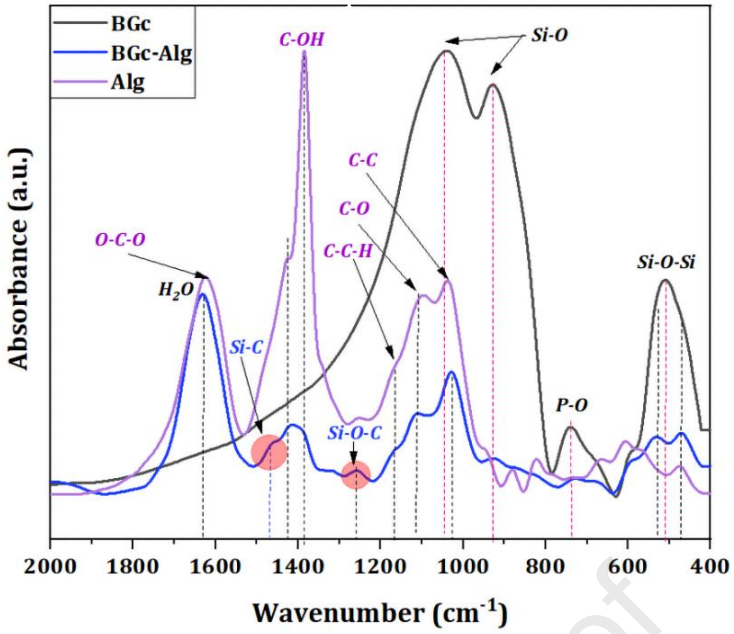

Figure 6. FTIR spectrum of BGc-Alg powder compared to Alg and BGc spectra.

3.1.3.2. Setting time

The setting time of the developed materials was investigated as a function of BG particle size and the nature of the liquid phase (Table 4). The setting time was considerably influenced by modifying the particle size and the liquid phase. The initial and final setting times of the formulated cement in the presence of distilled water increased significantly as the size of the integrated BG particles decreased. Indeed, the initial setting time for CPC-BGc was 50 ± 3 minutes, and the final setting time was 71 ± 4 minutes, whereas CPC-BGm increased to values of 75 ± 4 min and 91 ± 4 min, respectively, for the initial and final setting times. The cement prepared with the fine bioactive glass (BGf) had the slowest setting times, with an initial time of about 92 ± 4 min and a final time of 134 ± 5 min. The results obtained showed that in the presence of distilled water, the cement formulated with the coarse bioactive glass had the shortest setting times, followed by the CPC-BGm, and then CPC-BGf. This finding could be directly related to the setting reaction (apatite formation), which demonstrated that the CPC-BGc had the faster setting reaction. The increase of setting time by the reduction of BG particle size can be attributed to the slowing effect of Si ion (inhibitor of apatite formation) which is more abundant in formulations containing BGf as confirmed by ICP analysis.

The use of alginate hydrogel as a liquid phase reduced the setting time of composites made with BGf from 92 minutes to 64 minutes. The addition of alginate hydrogel, on the other hand, considerably increased the setting time of CPC-BGc from 50 to 82 minutes. Furthermore, it was demonstrated that the presence of the hydrogel did not affect the setting time of CPC-BGm, except for a minor decrease in the initial setting time. These findings are consistent with the trend found in the setting reaction, which indicates an accelerated setting reaction of CPC-BGm-Alg and CPC-BGf-Alg cements with Alg as the liquid phase. When the alginate was solubilized in the Na_2HPO_4 solution, the setting times for all formulated composite cements decreased significantly. Furthermore, it was found that the setting time increased as the BG particle size decreased. The values obtained for the initial setting time are 12 ± 2 min, 26 ± 4 min, 32 ± 4 min for CPC-BGc-Alg-NaP, CPC-BGm-Alg-NaP, and CPC-BGf-Alg-NaP composites, respectively. These values are in the range required for clinical application.

Table 4. Initial and final setting times of the prepared composites.

Materials	Initial setting time (min)	Final setting time (min)
CPC-BGc	50 ± 3	71 ± 4
CPC-BGm	75 ± 4	95 ± 4
CPC-BGf	92 ± 3	134 ± 5
CPC-BGc-Alg	82 ± 4	125 ± 5
CPC-BGm-Alg	71 ± 3	95 ± 3
CPC-BGf-Alg	64 ± 2	87 ± 3
CPC-BGc-Alg-NaP	10 ± 2	22 ± 4
CPC-BGm-Alg-NaP	26 ± 4	40 ± 4
CPC-BGf-Alg-NaP	32 ± 4	38 ± 4

3.1.3.3. SEM examination

The morphology of the hardened and dried cements was analyzed at 100 µm, to assess their surface and, in particular, to evaluate qualitatively their porosity (Figure 7). SEM images showed that the cements formulated with coarse bioactive glass present the densest structure

for the three liquid phases used. While materials prepared with medium (BGm) and fine (BGf) bioactive glass show porous structure and exhibited pores with different sizes. The use of Alg as a liquid phase in the presence of BG reduces the pores size and this effect becomes more pronounced in the presence of Alg-NaP as a liquid phase.

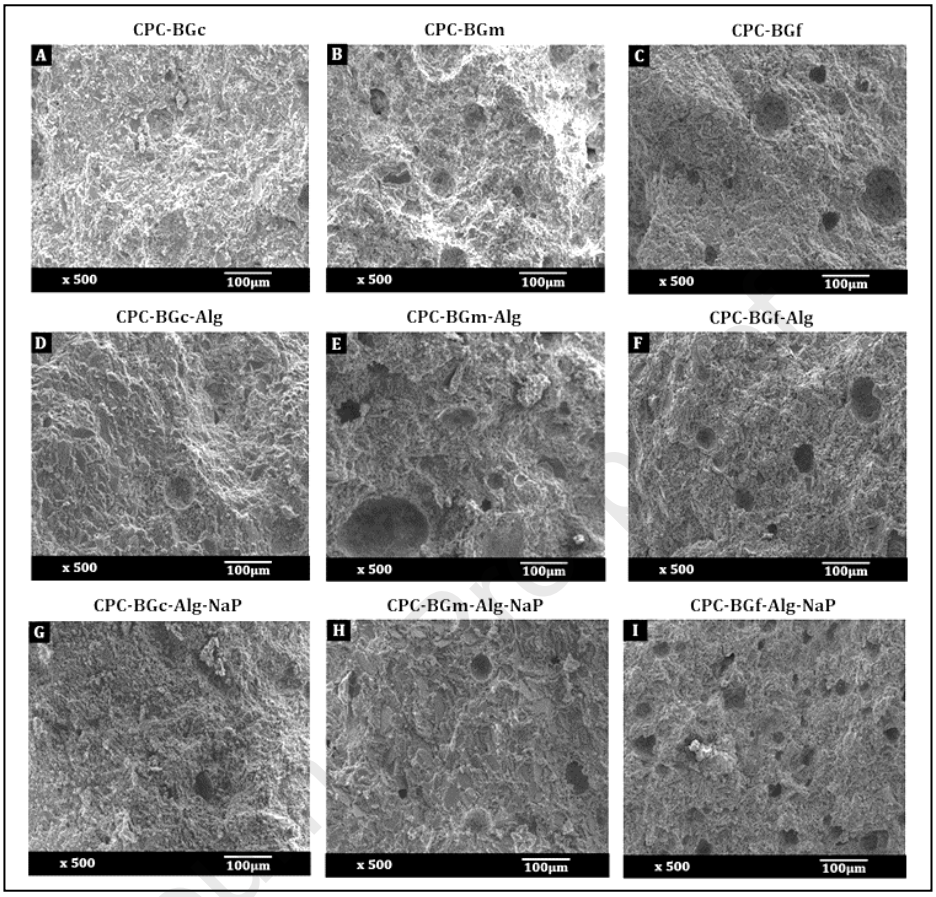

Figure 7. SEM micrographs at 100 µm of CPC-BGc (A), CPC-BGm (B), CPC-BGm (C), CPC-BGc-Alg (D), CPC-BGm-Alg (E), CPC-BGf-Alg (F), CPC-BGc-Alg-NaP (G), CPC-BGm-Alg-NaP (H), and CPC-BGf-Alg-NaP (I).

Figure 8 showed surface morphologies of all prepared materials at 2 µm. The SEM analysis of CPC-BGc, CPC-BGc-Alg, and CPC-BGc-Alg-NaP revealed the presence of tiny spherical particles, as well as blocky particles, respectively attributed to residual vaterite and bioactive glass surrounded by needle-like crystals of precipitated apatite. However, differences in the microstructure of the composites can be observed toward the particle size of the incorporated BG. It appears that the needle-shaped precipitated apatite crystals were more agglomerated, much larger in composites formulated with coarse BG particles. This observation confirmed

the high-intensity ratio observed for CPC-BGc, CPC-BGc-Alg, and CPC-BGc-Alg-NaP as confirmed by XRD diffraction. Moreover, the size of the precipitated crystals was significantly smaller in composites prepared with BGf. Similarly, Ginebra et al., reported that decreasing the particle size of α-TCP-based cement induced a decrease in the size of the formed apatite crystals [14].

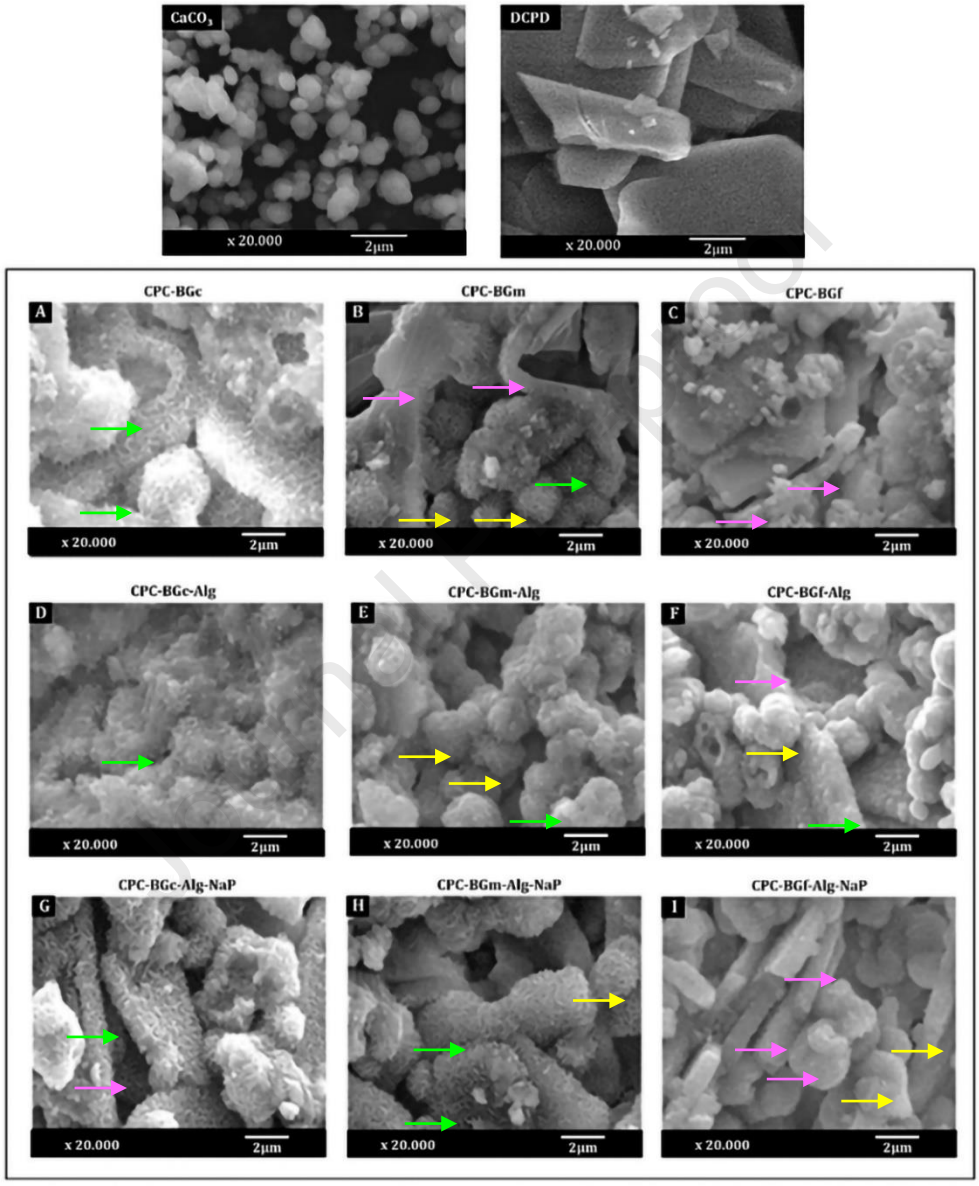

Figure 8. SEM micrographs at 2µm of CPC-BGc (A), CPC-BGm (B), CPC-BGf (C), CPC-BGc-Alg (D), CPC-BGm-Alg (E), CPC-BGf-Alg (F), CPC-BGc-Alg-NaP (G), and CPC-BGm-Alg-NaP (H), and CPC-BGm-Alg-NaP (I). (Yellow arrows: vaterite, pink arrows: bioactive glass, green arrows: apatite).

3.1.3.4. Cohesion and injectability properties

The cohesion ability of composite pastes was assessed regarding the particle size of BG and the nature of the liquid phase (figure 9). It should be noted that the cements CPC-BGf-Alg, CPC-BGf-Alg-NaP, and CPC-BGm-Alg-NaP have been shaped in cylindrical form as they are not injectable.

The photos were taken at 5 minutes and 24 hours after immersion in PBS solution and showed that the cohesion behavior depends on the BG particles size and the liquid phase used. In distilled water, the cement formulated with BGf (CPC-BGf) exhibited poorly cohesion presenting a total disintegration after 24 hours, while the CPC-BGc retained its shape and CPC-BGm was slightly affected. When alginate hydrogel is used as a liquid phase, the CPC-BGc-Alg composite exhibited an excellent cohesion, and the paste could harden without disintegrating into PBS solution. Moreover, CPC-BGm-Alg paste showed a good cohesion with the presence of small traces of turbidity when injected into the solution. However, the CPC-BGf-Alg composite showed a relatively poor cohesion, and the paste was disintegrating in the solution during the hardening process.

In the case of cements formulated with Alg-NaP as a liquid phase, the CPC-BGc-Alg-NaP and CPC-BGm-Alg-NaP composite cements showed good cohesion, while the CPC-BGf-Alg-NaP composite showed very low cohesion revealing that the paste started to disintegrate after 5 minutes of immersion in the PBS solution and complete disintegration after 24 hours.

In summary, the cohesion behavior of the prepared composites is strongly affected by the particle size of the BG regardless of the liquid phase used, indicating that composites formulated with coarse BGc particle size exhibited an excellent cohesion. The decrease of the BG particle size affected negatively the cohesion of the cement pastes. This effect could be due to the water absorption phenomenon. Indeed, the finer the particle size, the higher the water absorption, which increases the water demand for the cement with the fine BGf and consequently decreases the cohesion between the particles making up the cement. This effect appears to be less pronounced with the use of alginate hydrogel as the liquid phase. In

general, using viscous solutions as a liquid phase, such as polymeric gel, proved to be a useful method for improving CPC cohesion. Tanaka et al. investigated the anti-washout properties of Biopex® cement by adding sodium alginate into its liquid phase, and results revealed an improvement of the cohesion property due to the inhibition of water penetration in the cement pastes by the viscous gel of sodium alginate [44]. Furthermore, the use of the setting accelerator in the liquid phase of the CPC-BGf-Alg-NaP, on the other hand, affects its cohesiveness, and the paste disintegrates after 5 minutes of immersion. Regarding the effect of particle sizes, the results obtained in this work are not in agreement with findings reported in the literature [40,45]. It is known that generally, reducing the particle size of the bioactive glass powder is used as an approach to improve the cohesion of cement pastes. Bohner et al, conducted a theoretical and experimental investigation to assess the impact of various factors on the cohesion of calcium phosphate cement paste [46]. The findings of this study revealed that reducing the particle size of the reactive powders and using viscous solutions are the most effective methods for improving the cohesion of cement pastes.

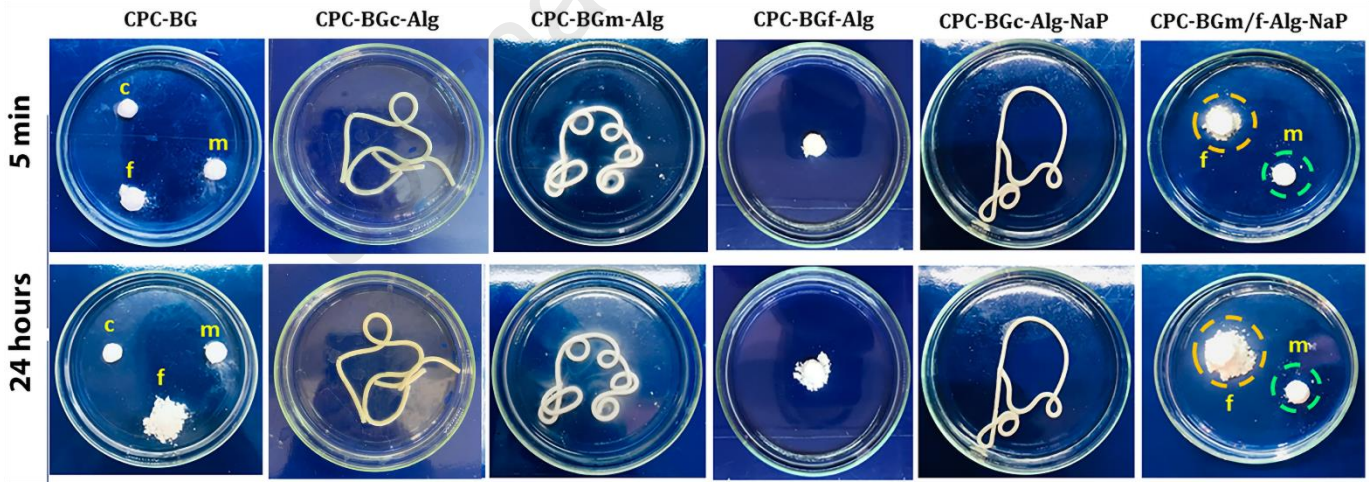

Figure 9. Photos of formulated pastes taken after 5 minutes and 24 hours of immersion in PBS solution (c: coarse, m: medium, and f: fine).

It is known that injectability is one of the most important properties of calcium phosphate cements and promotes their use for clinical application for minimally invasive surgery. This property is affected through parameters, such as the particle size of powders, liquid to powder ratio, nature of the liquid phase, compositions, etc. In the current study, the injectability

behavior is evaluated regarding the particle size of the bioactive glass 46S6 as a function of the liquid phase nature (Figure 10).

The results showed that the injectability of composites formulated was strongly affected by the BG particle size and the liquid phase. Indeed, it has been noted that the injectability decreased when the particle size of the bioactive glass is reduced. An injectability value of 62% was measured for the CPC-BGc cement, followed by CPC-BGm with a value of 48%, and the CPC-BGf cement that exhibited the lower value of approximately 26%. The decrease in BG particle size reduced the injectability of cement pastes prepared in distilled water which could be explained by particle agglomeration as well as increased water absorption by fine BG particles, causing an increase in frictional contact between particles [47]. These results are in accordance with those reported by Aberg et al. which evaluated the effect of particle size on hardening and handling of a premixed calcium phosphate cement-based on monocalcium phosphate hydrate (MCPH) with various particle size ranges (<100, 100–200, 200–400, and 400–600µm) and β-tricalcium phosphate (β-TCP) granules of particle size in the range of 150–500µm [15]. The obtained results attested that smaller particle sizes resulted in cements that exhibit higher extrusion forces and therefore a decrease of injectability[15]. Contrary to this tendency, other studies demonstrated that a decrease in the particle sizes of the constituents of calcium phosphate cements induces an increase in their injectability. Tadier et al. found that the injectability of pastes and putties, loaded with millimeter-sized glass beads, decreased with the increasing size of beads resulting in the formation of a percolation network that completely blocked the movement of the plunger and hindered further the extrusion [48].

Furthermore, the use of alginate hydrogel as a liquid phase increased the injectability of the CPC-BGc-Alg and CPC-BGm-Alg reaching injectability values of 98% and 76%, respectively. However, the addition of Alg to the CPC-BGf matrix decreased the injectability from a value of 26% down to 16%. Generally, the addition of polymers especially hydrogels in the CPC liquid phase resulted in an enhancement of the injectability of CPC pastes [49]. The increase in injectability with the use of hydrogel as the liquid phase for composites

prepared with coarse and medium glass could be due to the lubricating effect which could facilitate the sliding of the particles on each other and consequently facilitate their injection through the syringe. However, the decrease of injectability observed for the cement formulated with BGf in the presence of alginate hydrogel can be attributed to the increase of viscosity in the paste cement. Although, samples formulated with BGm and BGf in the presence of Alg-NaP hydrogel as the liquid phase (CPC-BGm-Alg-NaP and CPC-BGf-Alg-NaP) revealed a change in their injectability behavior. While the injectability of the composite formulated with BGc (CPC-BGc-Alg-NaP) was not affected. Indeed, the injectability percentage of CPC-BGc-Alg-NaP composite cement showed a value of 95 %, while the injectability critically decreased for CPC-BGm-Alg-NaP from a value of 76% down to 18%, and the CPC-BGf-Alg-NaP from a value of 16% down to 0%, and the composite cement became non-injectable. The drastic decrease in the injectability in the case of CPC-BGm-Alg-NaP and CPC-BGf-Alg-NaP could be attributed to the accelerated setting and hardening processes of composite cements by the addition of the setting solution (NaP) and water absorption phenomenon, which is more evident as the BG particle size decreased. Furthermore, the drop in injectability to 0% for the CPC-BGf-Alg-NaP composite could be due to the particles' agglomeration phenomenon, and consequently the increase of the friction contact.

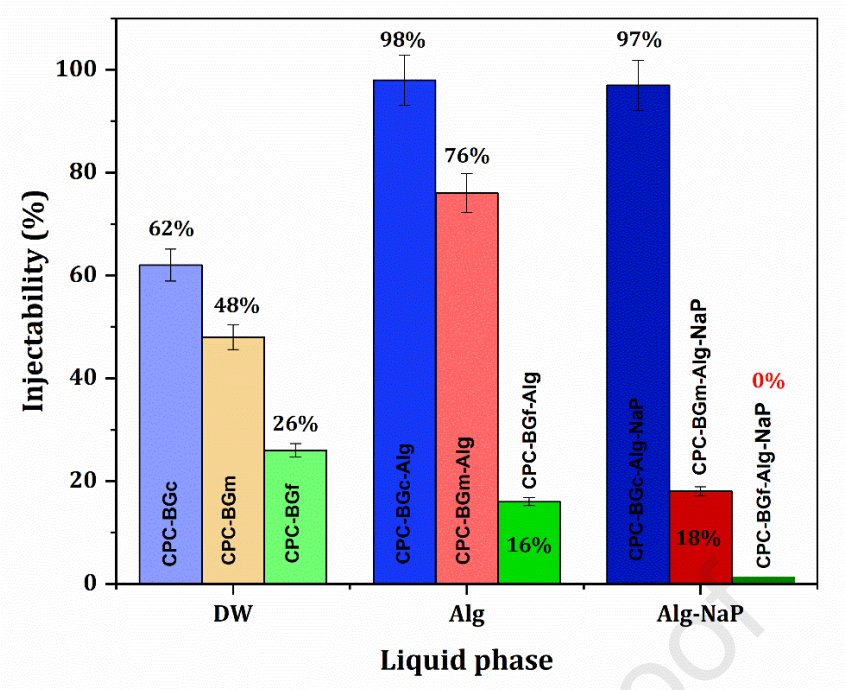

Figure 10. Injectability values of prepared materials regarding the BG particle size and the nature of the liquid phase.

3.1.3.5. Compressive strength

The compressive strength values of all prepared specimens were measured and illustrated in figure 11. The obtained results showed that the compressive strength depends on the liquid phase used and the particle size. Indeed, as the particle size of BG is coarse, the compressive strength reached its maximum for all liquid phases used. In distilled water, the compressive strength of CPC-BGc cement was 5.8MPa and decreased with reducing the BG particle size down to a value of 3.5MPa and 3.1MPa for CPC-BGm and CPC-BGf cements, respectively. The same trend was observed when the sodium alginate is used as a liquid phase, showing a decrease of the compressive strength from a value of 7.4MPa for CPC-BGc-Alg composite down to 4.6MPa and 4.1MPa for CPC-BGm-Alg and CPC-BGf-Alg composites, respectively. For the formulations in the presence of Alg-NaP hydrogel as a liquid phase, the compressive strength reached a maximum value of 10.5MPa for CPC-BGc-Alg-NaP which decreased down to 5.2MPa and 3.3 for CPC-BGm-Alg-NaP and CPC-BGf-Alg-NaP composites, respectively.

The results showed that as the size of the bioactive glass was reduced, the compressive strength decreased significantly. This could be explained by the reduced cohesion of cement pastes using fine glass (BGf), as well as the lower apatite content compared to the other composites as confirmed by XRD analysis. Indeed, the lack of cohesion between the particles in cements produced with BGf would preclude intimate contact between them, eliminating the binding action of the alginate, thus, lowering compressive strength. Furthermore, the intensity ratio (I_A/I_V) dropped when the size of the BG was reduced. In fact, for formulations including BGc, the cements have superior intensity ratios than formulations containing BGm and BGf. This drop could influence the production of apatite crystals, which filled voids and reduced the inter-particle distance, resulting in a denser and compact network. Contrary to the results obtained, Ginebra et al, investigated the effect of the particle size of the powder phase on the mechanical resistance of the α-tricalcium phosphate (α-TCP) system [40]. The obtained results revealed the increase in the compressive strength at the early stage with decreasing the particle size of starting powders. Otsuka et al. investigated a system for delivering antibiotics using a self-setting CPC comprising DCPD/TTCP, concluding that the particle sizes of DCPD and TTCP impacted the compressive strength, the smaller the particle size was, the higher the cement strength was, this effect was related to the nucleation and crystal growth processes during the setting phase [50].

Concerning the effect of the liquid phase, it was found that the use of sodium alginate increased the compressive strength of the materials prepared with the three BG particle sizes (BGc, BGm, and BGf) compared to that prepared with distilled water. This effect could be related to the decrease of porosity as shown in SEM examination and also the formation of calcium alginate compound which acted as a reinforcing agent for cements matrix. Indeed, several studies have shown that the use of biopolymers in the liquid phase increases the mechanical properties of calcium phosphate cements [12]. Sprio et al., showed that the addition of sodium alginate to the cement-based on the Sr-substituted α-TCP led to an increase in the compressive strength and this was attributed to a crack-bridging effect

provided by alginate [24]. It has been reported by Jacquart et al, that the use of carboxymethylcellulose with DCPD-$CaCO_3$ cement significantly enhanced the compressive strength of formulated composites [51]. The use of sodium phosphate solution for the preparation of alginate gel resulted in an increase of compressive strength of cements formulated with BGc and BGm (CPC-BGc-Alg-NaP and CPC-BGm-Alg-NaP). This effect could be attributed to the reaction between Ca of residual vaterite and P of the NaP, which may promote the formation and growth of apatite crystals that fill the pores observed when used distilled water and alginate solution. This allows the densification of the cement structure as confirmed by SEM examination. As a conclusion, the values of compressive strength for all formulated composite cements are in the range of 3 to 10.5 MPa, which are similar to that of cancellous bone [52].

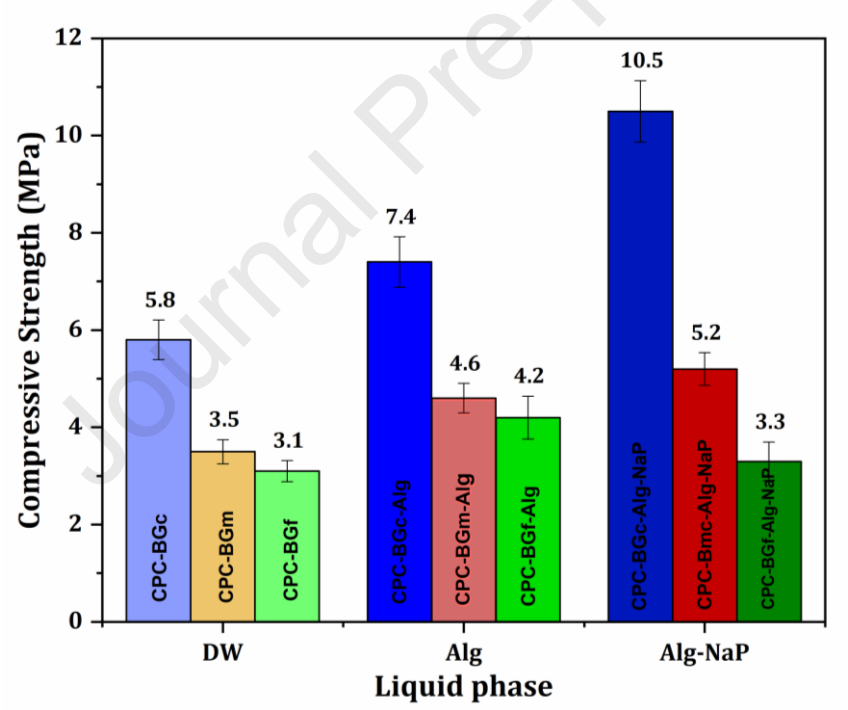

Figure 11. Compressive strength of prepared cement composites, as a function of BG particle size and the liquid phase nature.

3. Conclusion

In this study, the effect of BG particle size and the nature of the liquid phase on calcium phosphate properties was investigated in terms of setting reaction, microstructure, setting

time, injectability, cohesion, and compressive strength. The modification of the particle size of the bioactive glass altered the kinetics of the setting, handling, and mechanical properties of the prepared cements. The setting reaction was critically modified during the first hours depending on the BG particle size and liquid phase. The cement prepared with coarse particle size demonstrated the best characteristics in terms of setting time, which is around 12min, thus fulfilling clinician requirement. Furthermore, the injectability of these types of cements is almost 95%, showing good cohesion and enhanced mechanical strength (10.5 MPa). The final material elaborated in the presence of BGc, and alginate solubilized in the setting accelerator (CPC-BGc-Alg-NaP) could be a potentially composite cement for no-load bearing applications and minimally invasive surgery. The poor injectability and cohesion of CPC-BGm-Alg-NaP and CPC-BGf-Alg-NaP composite cements hinder their application as injectable pastes; nevertheless, they could be exploited as hardened cements in the form of implantable blocks for orthopedic applications.

Acknowledgment

This work was carried out with the financial support of the OCP group (Morocco) through the APPHOS Program (project ID: MAT-BAR-01/ 2017). The authors further thank the Center of Analysis and Characterization Center (CAC) of Cadi Ayyad University. We would like also to thank especially Pr Rachid HAKKOU for Mechanical properties and ICP analysis.

Reference

[1] P.W. Brown, L.C. Chow, A new calcium phosphate, water-setting cement, Cem. Res. Progress,. (1987) 352–379.

[2] R.Z. LeGeros, Calcium phosphate materials in restorative dentistry: a review., Adv. Dent. Res. 2 (1988) 164–180. https://doi.org/10.1177/08959374880020011101.

[3] A.M. Yousefi, A review of calcium phosphate cements and acrylic bone cements as injectable materials for bone repair and implant fixation, J. Appl. Biomater. Funct. Mater. 17 (2019). https://doi.org/10.1177/2280800019872594.

[4] C. Combes, R. Bareille, C. Rey, I. U-, L. Biomate, Calcium carbonate – calcium phosphate mixed cement compositions for bone reconstruction, (2006). https://doi.org/10.1002/jbm.a.

[5] B. Myszka, K. Hurle, K. Zheng, S.E. Wolf, A.R. Boccaccini, Mechanical improvement of calcium carbonate cements by: In situ HEMA polymerization during hardening, J. Mater. Chem. B. 7 (2019) 3403–3411. https://doi.org/10.1039/c9tb00237e.

[6] C. Combes, B. Miao, R. Bareille, C. Rey, Preparation, physical-chemical characterisation and cytocompatibility of calcium carbonate cements, Biomaterials. 27 (2006) 1945–1954. https://doi.org/10.1016/j.biomaterials.2005.09.026.

[7] D. Yang, Y. Yan, X. Liu, P. Wang, G. Huang, G. Xu, G. Sun, D. He, Characterization of an α-calcium sulfate hemihydrates/α-tricalcium phosphate combined injectable bone cement, ACS Appl. Bio Mater. 1 (2018) 768–776. https://doi.org/10.1021/acsabm.8b00221.

[8] H. Mabroum, H. Noukrati, H. Ben youcef, B. Lefeuvre, H. Oudadesse, A. Barroug, Physicochemical, setting, rheological, and mechanical properties of a novel bio-composite based on apatite cement, bioactive glass, and alginate hydrogel, Ceram. Int. (2021). https://doi.org/10.1016/j.ceramint.2021.05.106.

[9] A.C. Renno, F.C. van de Watering, M.R. Nejadnik, M.C. Crovace, E.D. Zanotto, J.G.

Wolke, J.A. Jansen, J.J. van den Beucken, Incorporation of bioactive glass in calcium phosphate cement: An evaluation, Acta Biomater. 9 (2013) 5728–5739. https://doi.org/10.1016/j.actbio.2012.11.009.

[10] L. Yu, Y. Li, K. Zhao, Y. Tang, Z. Cheng, J. Chen, Y. Zang, J. Wu, L. Kong, S. Liu, W. Lei, Z. Wu, A novel injectable calcium phosphate cement-bioactive glass composite for bone regeneration, PLoS One. 8 (2013) e62570. https://doi.org/10.1371/journal.pone.0062570.

[11] A.C.M. Renno, M.R. Nejadnik, F.C.J. Van De Watering, M.C. Crovace, E.D. Zanotto, J.P.M. Hoefnagels, J.G.C. Wolke, J.A. Jansen, J.J.J.P. Van Den Beucken, Incorporation of bioactive glass in calcium phosphate cement: Material characterization and in vitro degradation, J. Biomed. Mater. Res. - Part A. 101 A (2013) 2365–2373. https://doi.org/10.1002/jbm.a.34531.

[12] R.A. Perez, H.W. Kim, M.P. Ginebra, Polymeric additives to enhance the functional properties of calcium phosphate cements, J. Tissue Eng. 3 (2012) 1–20. https://doi.org/10.1177/2041731412439555.

[13] M.P. Ginebra, F.C.M. Driessens, J.A. Planell, Effect of the particle size on the micro and nanostructural features of a calcium phosphate cement: A kinetic analysis, Biomaterials. 25 (2004) 3453–3462. https://doi.org/10.1016/j.biomaterials.2003.10.049.

[14] M.P. Ginebra, F.C.M. Driessens, J.A. Planell, Effect of the particle size on the micro and nanostructural features of a calcium phosphate cement: A kinetic analysis, Biomaterials. 25 (2004) 3453–3462. https://doi.org/10.1016/j.biomaterials.2003.10.049.

[15] J. Åberg, J. Engstrand, H. Engqvist, Influence of particle size on hardening and handling of a premixed calcium phosphate cement, J. Mater. Sci. Mater. Med. 24 (2013) 829–835. https://doi.org/10.1007/s10856-013-4855-z.

[16] J. Zhang, W. Liu, V. Schnitzler, F. Tancret, J.M. Bouler, Calcium phosphate cements for bone substitution: Chemistry, handling and mechanical properties, Acta Biomater. 10 (2014) 1035–1049. https://doi.org/10.1016/j.actbio.2013.11.001.

[17] A. El-Fiqi, J.H. Kim, R.A. Perez, H.W. Kim, Novel bioactive nanocomposite cement formulations with potential properties: incorporation of the nanoparticle form of mesoporous bioactive glass into calcium phosphate cements, J. Mater. Chem. B. 3 (2015) 1321–1334. https://doi.org/10.1039/c4tb01634c.

[18] Y. Huang, J. Zhang, W. Zhang, S. Zeng, H. Shi, T. Yu, C. Zhou, Formulation of α-Tricalcium Phosphate Bone Cement Based on an Alginate-Chitosan Gel System, Cryst. Growth Des. 20 (2020) 1400–1404. https://doi.org/10.1021/acs.cgd.0c00005.

[19] W.J.E.M. Habraken, H.B. Liao, Z. Zhang, J.G.C. Wolke, D.W. Grijpma, A.G. Mikos, J. Feijen, J.A. Jansen, In vivo degradation of calcium phosphate cement incorporated into biodegradable microspheres, Acta Biomater. 6 (2010) 2200–2211. https://doi.org/10.1016/j.actbio.2009.12.028.

[20] L.P. Silva, M.D.P. Ribeiro, E.S. Trichês, M. Motisuke, Brushite cement containing gelatin: Evaluation of mechanical strength and in vitro degradation, Ceramica. 65 (2019) 261–266. https://doi.org/10.1590/0366-69132019653742585.

[21] W. Liu, J. Zhang, P. Weiss, F. Tancret, J.M. Bouler, The influence of different cellulose ethers on both the handling and mechanical properties of calcium phosphate cements for bone substitution, Acta Biomater. 9 (2013) 5740–5750. https://doi.org/10.1016/j.actbio.2012.11.020.

[22] G.S. Lee, J.H. Park, J.E. Won, U.S. Shin, H.W. Kim, Alginate combined calcium phosphate cements: Mechanical properties and in vitro rat bone marrow stromal cell responses, J. Mater. Sci. Mater. Med. 22 (2011) 1257–1268. https://doi.org/10.1007/s10856-011-4296-5.

[23] K.Y. Lee, D.J. Mooney, Alginate: Properties and biomedical applications, Prog. Polym.

Sci. 37 (2012) 106–126. https://doi.org/10.1016/j.progpolymsci.2011.06.003.

[24] S. Sprio, M. Dapporto, M. Montesi, S. Panseri, W. Lattanzi, E. Pola, G. Logroscino, A. Tampieri, Novel osteointegrative sr-substituted apatitic cements enriched with Alginate, Materials (Basel). 9 (2016) 1–17. https://doi.org/10.3390/ma9090763.

[25] M. Drahansky, M.. Paridah, A. Moradbak, A.. Mohamed, F. abdulwahab taiwo Owolabi, M. Asniza, S.H.. Abdul Khalid, We are IntechOpen , the world ' s leading publisher of Open Access books Built by scientists , for scientists TOP 1 %, Intech. i (2016) 13. https://doi.org/http://dx.doi.org/10.5772/57353.

[26] Y. guang Bi, Z. ting Lin, S. ting Deng, Fabrication and characterization of hydroxyapatite/sodium alginate/chitosan composite microspheres for drug delivery and bone tissue engineering, Mater. Sci. Eng. C. 100 (2019) 576–583. https://doi.org/10.1016/j.msec.2019.03.040.

[27] S. Srinivasan, R. Jayasree, K.P. Chennazhi, S. V Nair, R. Jayakumar, Biocompatible alginate / nano bioactive glass ceramic composite scaffolds for periodontal tissue regeneration, Carbohydr. Polym. 87 (2012) 274–283. https://doi.org/10.1016/j.carbpol.2011.07.058.

[28] K. Ishikawa, Y. Miyamoto, M. Kon, M. Nagayama, K. Asaoka, Non-decay type fast-setting calcium phosphate cement: composite with sodium alginate, Biomaterials. 16 (1995) 527–532. https://doi.org/10.1016/0142-9612(95)91125-I.

[29] S. Sprio, M. Dapporto, M. Montesi, S. Panseri, W. Lattanzi, E. Pola, G. Logroscino, A. Tampieri, Novel Osteointegrative Sr-Substituted Apatitic Cements Enriched with Alginate, Mater. 9 (2016). https://doi.org/10.3390/ma9090763.

[30] A. Sadiasa, S.K. Sarkar, R.A. Franco, Y.K. Min, B.T. Lee, Bioactive glass incorporation in calcium phosphate cement-based injectable bone substitute for improved in vitro biocompatibility and in vivo bone regeneration, J. Biomater. Appl. 28 (2014) 739–756. https://doi.org/10.1177/0885328213478256.

[31] A.C.M. Renno, F.C.J. Van De Watering, M.R. Nejadnik, M.C. Crovace, E.D. Zanotto, J.G.C. Wolke, J.A. Jansen, J.J.J.P. Van Den Beucken, Incorporation of bioactive glass in calcium phosphate cement: An evaluation, Acta Biomater. 9 (2013) 5728–5739. https://doi.org/10.1016/j.actbio.2012.11.009.

[32] H. Noukrati, S. Cazalbou, I. Demnati, C. Rey, A. Barroug, C. Combes, Injectability, microstructure and release properties of sodium fusidate-loaded apatitic cement as a local drug-delivery system, Mater. Sci. Eng. C. 59 (2016) 177–184. https://doi.org/10.1016/j.msec.2015.09.070.

[33] H. Oudadesse, E. Dietrich, Y.L. Gal, P. Pellen, B. Bureau, A.A. Mostafa, G. Cathelineau, Apatite forming ability and cytocompatibility of pure and Zn-doped bioactive glasses, Biomed Mater. 6 (2011) 35006. https://doi.org/10.1088/1748-6041/6/3/035006.

[34] M. Mabrouk, A.A. Mostafa, H. Oudadesse, A.A. Mahmoud, M.I. El-Gohary, Bioactivity and drug delivering ability of a chitosan/46S6 melted bioactive glass biocomposite scaffold, InterCeram Int. Ceram. Rev. 62 (2013) 444–452.

[35] C. Combes, R. Bareille, C. %J J. of B.M.R.P.A.A.O.J. of T.S. for B. Rey The Japanese Society for Biomaterials, T.A.S. for Biomaterials, the K.S. for Biomaterials, Calcium carbonate–calcium phosphate mixed cement compositions for bone reconstruction, 79 (2006) 318–328.

[36] E. Fiume, J. Barberi, E. Verne, F. Baino, Bioactive Glasses: From Parent 45S5 Composition to Scaffold-Assisted Tissue-Healing Therapies, J Funct Biomater. 9 (2018). https://doi.org/10.3390/jfb9010024.

[37] L.L. Hench, J.R. Jones, Bioactive Glasses: Frontiers and Challenges, Front Bioeng Biotechnol. 3 (2015) 194. https://doi.org/10.3389/fbioe.2015.00194.

[38] F. Baino, S. Hamzehlou, S. Kargozar, Bioactive Glasses: Where Are We and Where Are We Going?, J Funct Biomater. 9 (2018). https://doi.org/10.3390/jfb9010025.

[39] M. Bohner, T.J. Brunner, W.J. Stark, Controlling the reactivity of calcium phosphate cements, J. Mater. Chem. 18 (2008) 5669–5675. https://doi.org/10.1039/b811953h.

[40] M.P. Ginebra, F.C. Driessens, J.A. Planell, Effect of the particle size on the micro and nanostructural features of a calcium phosphate cement: a kinetic analysis, Biomaterials. 25 (2004) 3453–3462. https://doi.org/10.1016/j.biomaterials.2003.10.049.

[41] C.L. Camire, S.J. Saint-jean, C. Mochales, P. Nevsten, J. Wang, L. Lidgren, I. Mccarthy, M. Ginebra, Material Characterization and In Vivo Behavior of Silicon Substituted ⎵ -Tricalcium Phosphate Cement, (2005) 424–431. https://doi.org/10.1002/jbm.b.30385.

[42] L. Corporation, A. Chemistry, B. Technology, Effects of Silicate Ions on the Formation and Transformation of Calcium Phosphates in Neutral Aqueous Solutions, 91 (1995) 3499–3503.

[43] S. Wang, X. Huang, M. Elimelech, Complexation between dissolved silica and alginate molecules : Implications for reverse osmosis membrane fouling, J. Memb. Sci. 605 (2020) 118109. https://doi.org/10.1016/j.memsci.2020.118109.

[44] S. Tanaka, T. Kishi, R. Shimogoryo, S. Matsuya, K. Ishikawa, Biopex® acquires anti-washout properties by adding sodium alginate into its liquid phase, Dent. Mater. J. 22 (2003) 301–312. https://doi.org/10.4012/dmj.22.301.

[45] M. Bohner, N. Doebelin, G. Baroud, Theoretical and experimental approach to test the cohesion of calcium phosphate pastes, Eur. Cells Mater. 12 (2006) 26–35. https://doi.org/10.22203/eCM.v012a03.

[46] M. Bohner, N. Doebelin, G. Baroud, Theoretical and experimental approach to test the cohesion of calcium phosphate pastes, Eur. Cells Mater. 12 (2006) 26–35. https://doi.org/10.22203/eCM.v012a03.

[47] R. O'Neill, H.O. McCarthy, E.B. Montufar, M.P. Ginebra, D.I. Wilson, A. Lennon, N. Dunne, Critical review: Injectability of calcium phosphate pastes and cements, Acta

Biomater. 50 (2017) 1–19. https://doi.org/10.1016/j.actbio.2016.11.019.

[48] S. Tadier, L. Galea, B. Charbonnier, G. Baroud, M. Bohner, Phase and size separations occurring during the injection of model pastes composed of β-tricalcium phosphate powder, glass beads and aqueous solutions, Acta Biomater. 10 (2014) 2259–2268. https://doi.org/10.1016/j.actbio.2013.12.018.

[49] R.A. Perez, H. Kim, M. Ginebra, Polymeric additives to enhance the functional properties of calcium phosphate cements, (2012). https://doi.org/10.1177/2041731412439555.

[50] M. Otsuka, Y. Suma, J.L. Fox, Y. Matsuda, W.I. Higuchi, Particle size effect of metastable calcium phosphates on crushing strength of self-setting bioactive calcium phosphate cement, Chem. Pharm. Bull. 41 (1993) 2055–2057. https://doi.org/10.1248/cpb.41.2055.

[51] S. Jacquart, D. Poquillon, G. Dechambre, S. Cazalbou, C. Rey, C. Combes, Mechanical properties of self-setting composites: influence of the carboxymethylcellulose content and hydration state, J. Mater. Sci. 51 (2016) 4296–4305. https://doi.org/10.1007/s10853-016-9739-4.

[52] A.J. Wagoner Johnson, B.A. Herschler, A review of the mechanical behavior of CaP and CaP/polymer composites for applications in bone replacement and repair, Acta Biomater. 7 (2011) 16–30. https://doi.org/10.1016/j.actbio.2010.07.012.

Lists of tables and figures

Table 1. Various formulations of the composite cements

Samples	Solid phase				Liquid phase	L/P
	$CaCO_3$ (wt %)	DCPD (wt %)	BG			
			wt %	particle size (µm)		
CPC-BGf	37.5	37.5	25	≤ 40	Distilled Water	0.7
CPC-BGm				40-100		
CPC-BGc				100-200		
CPC-BGf-Alg				≤ 40	5 wt % Alg in H_2O	
CPC-BGm-Alg				40-100		
CPC-BGc-Alg				100-200		
CPC-BGf-Alg-NaP				≤ 40	5 wt % Alg in Na_2HPO_4 (0.25 M)	
CPC-BGm-Alg-NaP				40-100		
CPC-BGc-Alg-NaP				100-200		

Table 2. Particle-size distribution parameters of the BG powders.

Bioactive glass	D (10) (µm)	Median Size, D (50) (µm)	D (90) (µm)	Particle size volume average, Mv (µm)
BGc	131 ± 5	198 ± 8	295 ± 12	207 ± 8
BGm	48 ± 2	81 ± 3	172 ± 7	90 ± 4
BGf	15 ± 1	20 ± 1	47 ± 2	23 ± 1

Table 3. ICP results of solutions containing BGc, BGm, and BGf.

Materials	Ca (mg/L)	Si (mg/L)
BGc-DW	0.05 ± 0.003	0.53 ± 0.03
BGm-DW	0.26 ± 0.02	1.42 ± 0.08
BGf-DW	0.81 ± 0.05	2.83 ± 0.17
BGc-Alg	5.16 ± 0.31	4.15 ± 0.25
BGm-Alg	5.18 ± 0.31	5.91 ± 0.35
BGf-Alg	5.54 ± 0.33	7.46 ± 0.44

Table 4. Initial and final setting times of the prepared composites.

Materials	Initial setting time (min)	Final setting time (min)
CPC-BGc	50 ± 3	71 ± 4
CPC-BGm	75 ± 4	95 ± 4
CPC-BGf	92 ± 3	134 ± 5
CPC-BGc-Alg	82 ± 4	125 ± 5
CPC-BGm-Alg	71 ± 3	95 ± 3
CPC-BGf-Alg	64 ± 2	87 ± 3
CPC-BGc-Alg-NaP	10 ± 2	22 ± 4
CPC-BGm-Alg-NaP	26 ± 4	40 ± 4
CPC-BGf-Alg-NaP	32 ± 4	38 ± 4

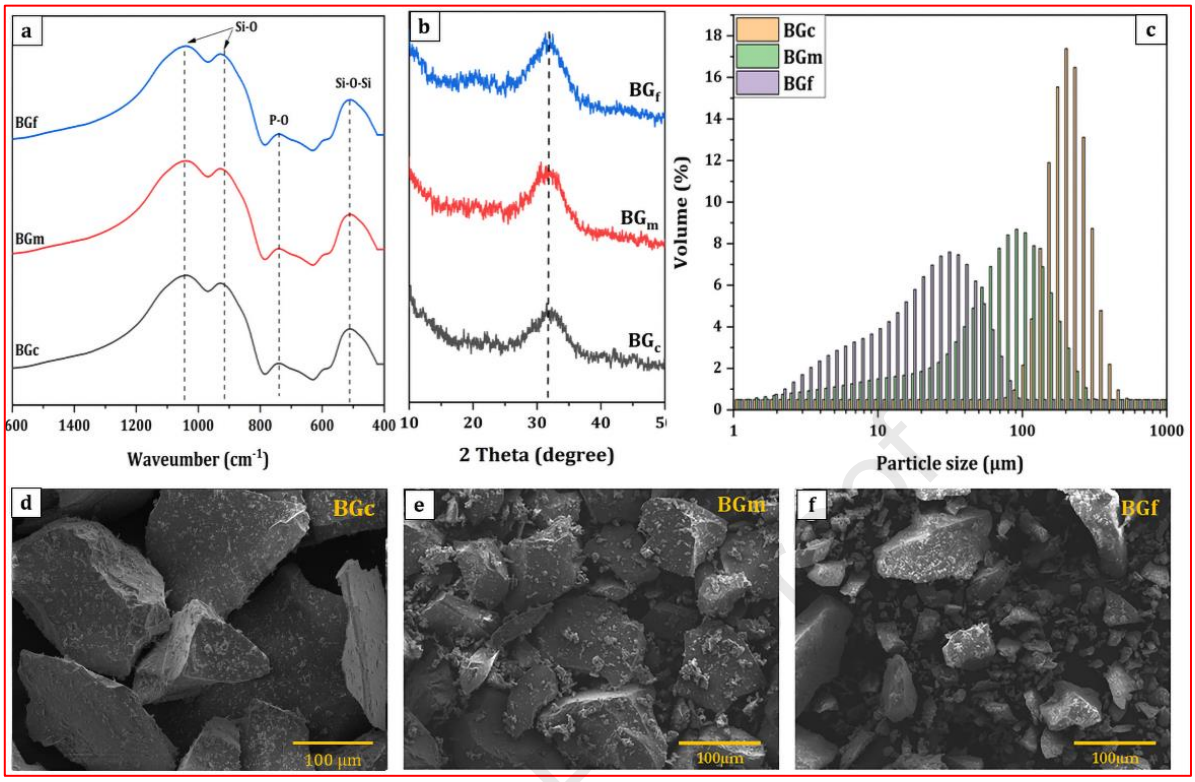

Figure 1. FTIR (a) and XRD (b), particle size distribution (c), and SEM micrographs of BGc (d), BGm (e), and BGf (f) of the bioactive glass 46S6 powder.

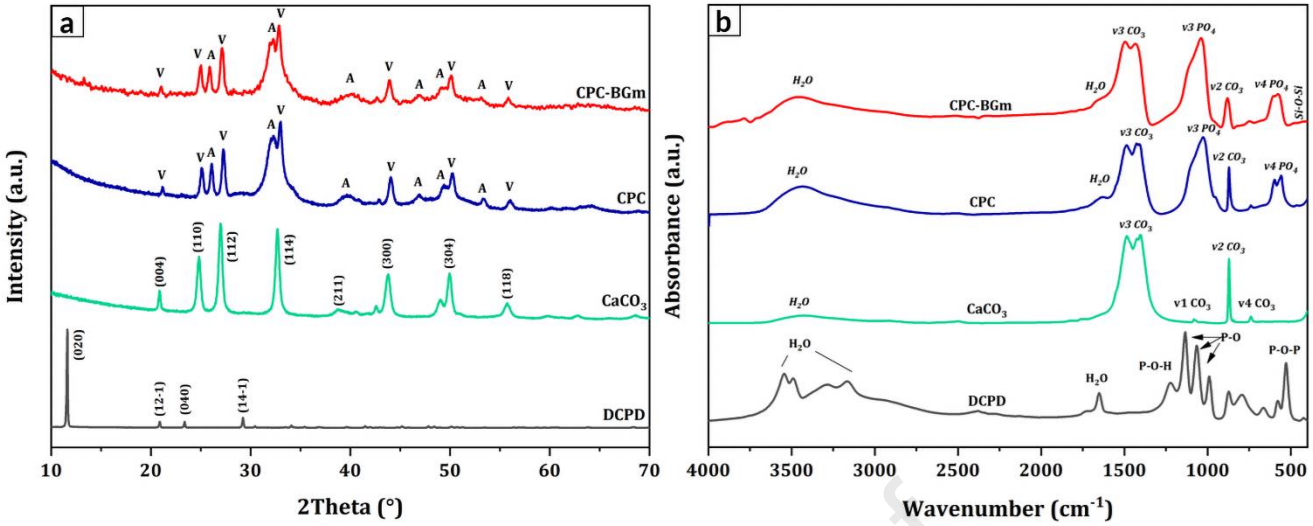

Figure 2. XRD patterns (a) and FTIR spectra (b) of CPC and CPC-BGm compared to the DCPD and $CaCO_3$ phases (A: Apatite, V: Vaterite).

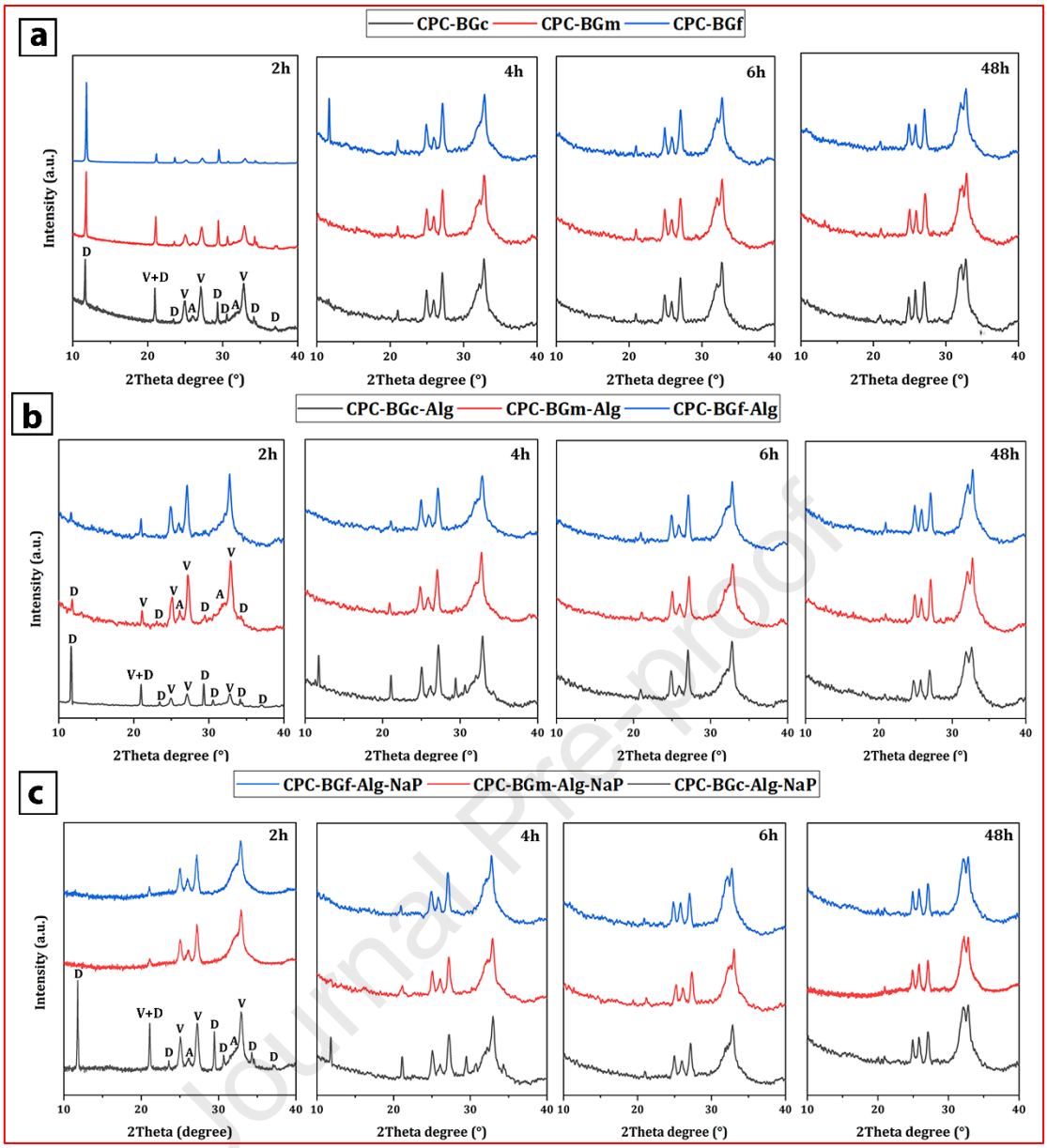

Figure 3. XRD patterns of the formulated materials as a function of reaction time, in distilled water (a), alginate hydrogel (b), and alginate with NaP (c); (D: DCPD, V: $CaCO_3$ and A: Apatite)

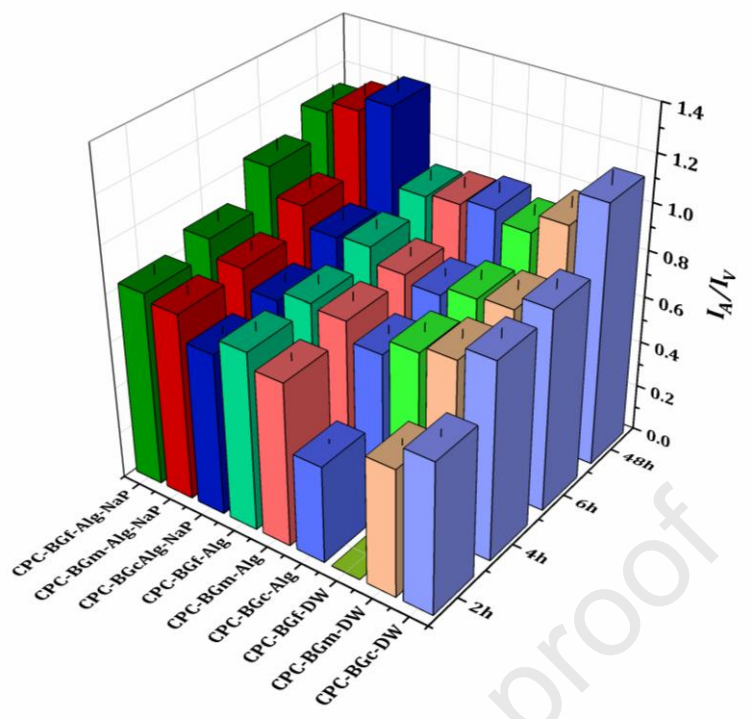

Figure 4. Intensity ratio (I_A/I_V) obtained from the XRD patterns of prepared materials as a function of incubation time.

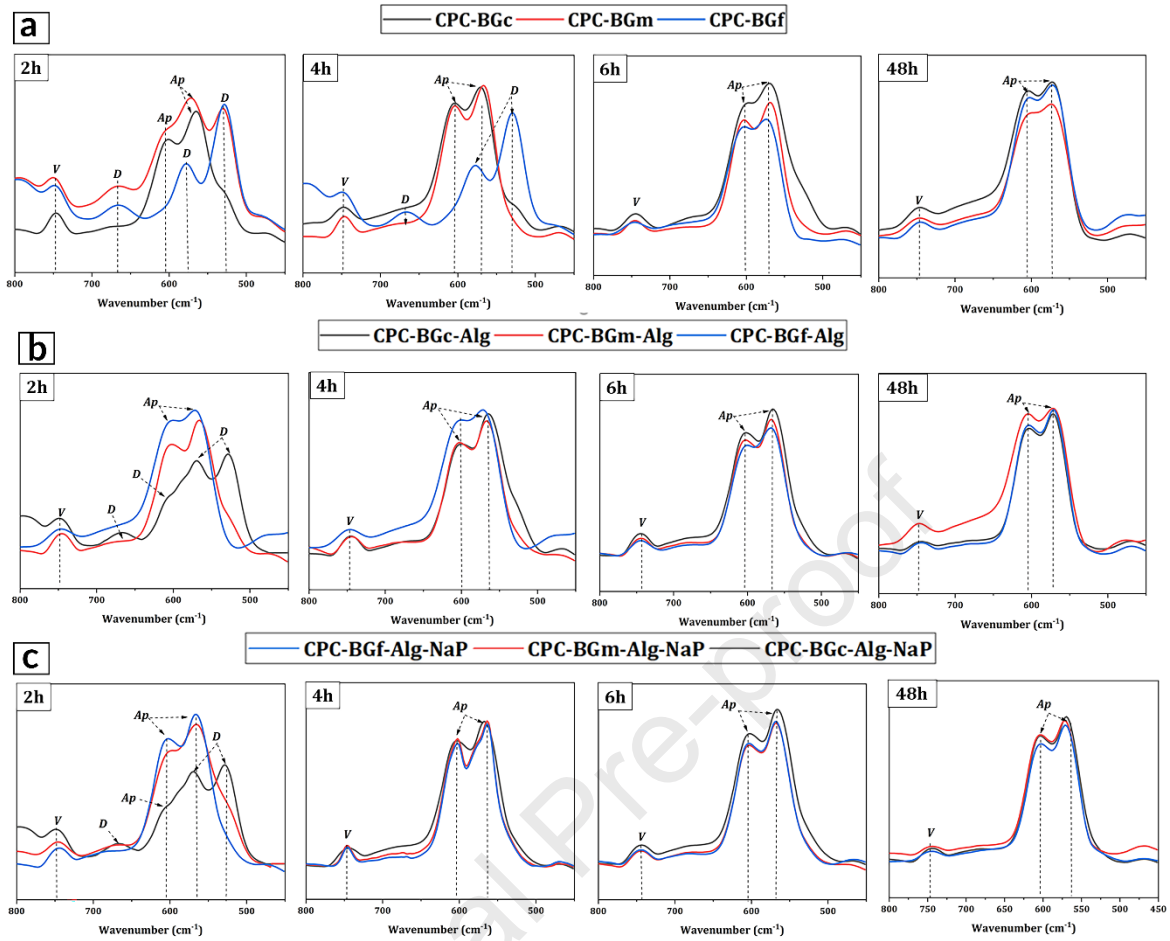

Figure 5. FTIR spectra of formulated materials in distilled water (a), alginate hydrogel (b), and Alg-NaP gel (c).

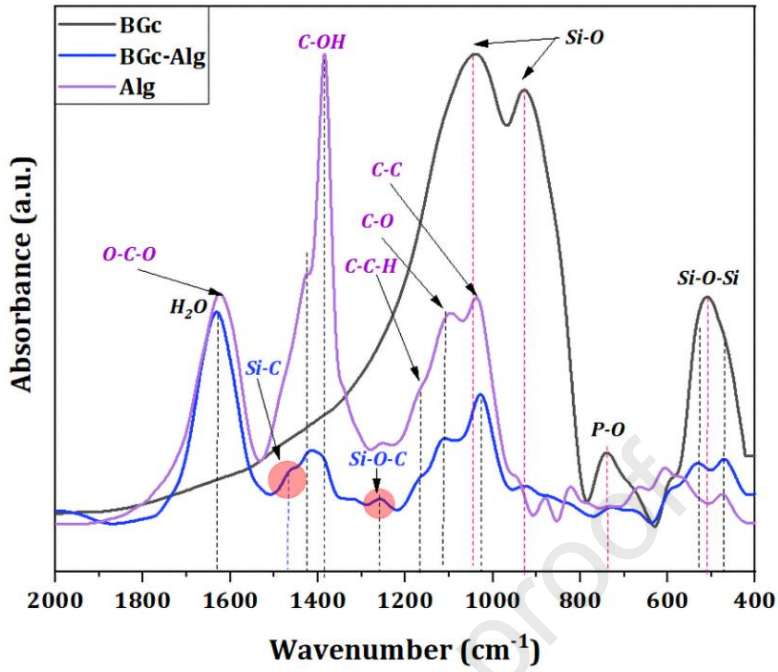

Figure 6. FTIR spectrum of BGc-Alg powder compared to Alg and BGc spectra.

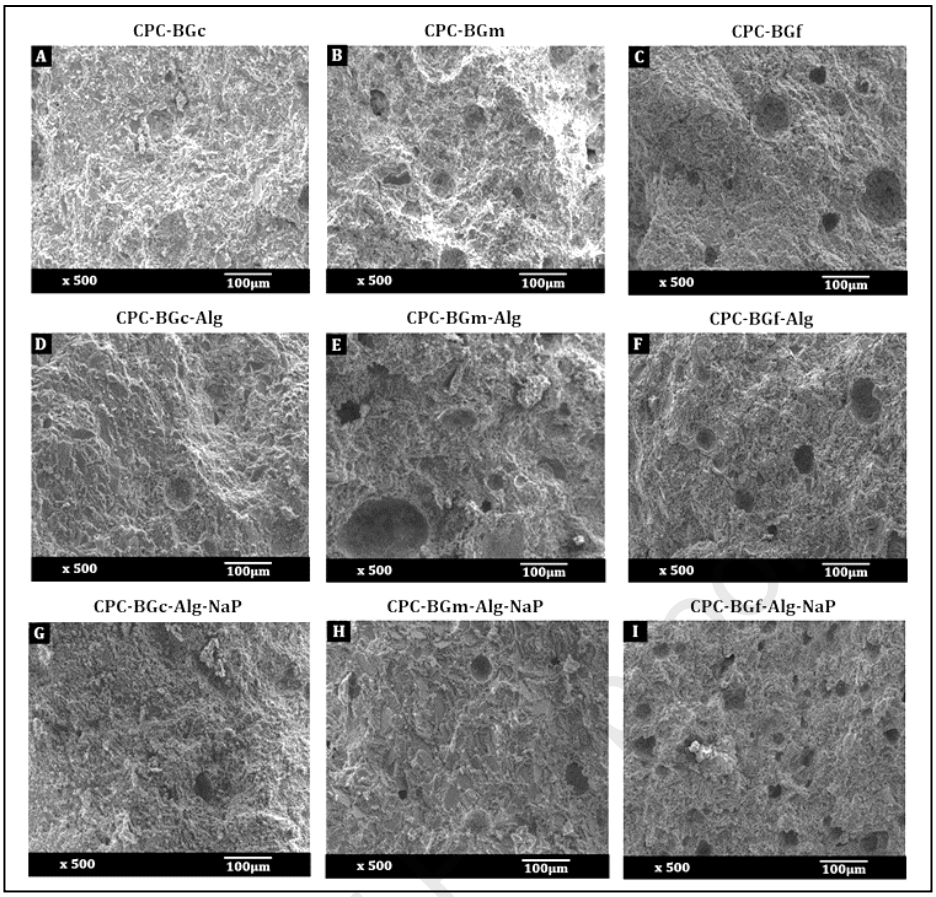

Figure 7. SEM micrographs at 100 µm of CPC-BGc (A), CPC-BGm (B), CPC-BGm (C), CPC-BGc-Alg (D), CPC-BGm-Alg (E), CPC-BGf-Alg (F), CPC-BGc-Alg-NaP (G), CPC-BGm-Alg-NaP (H), and CPC-BGf-Alg-NaP (I).

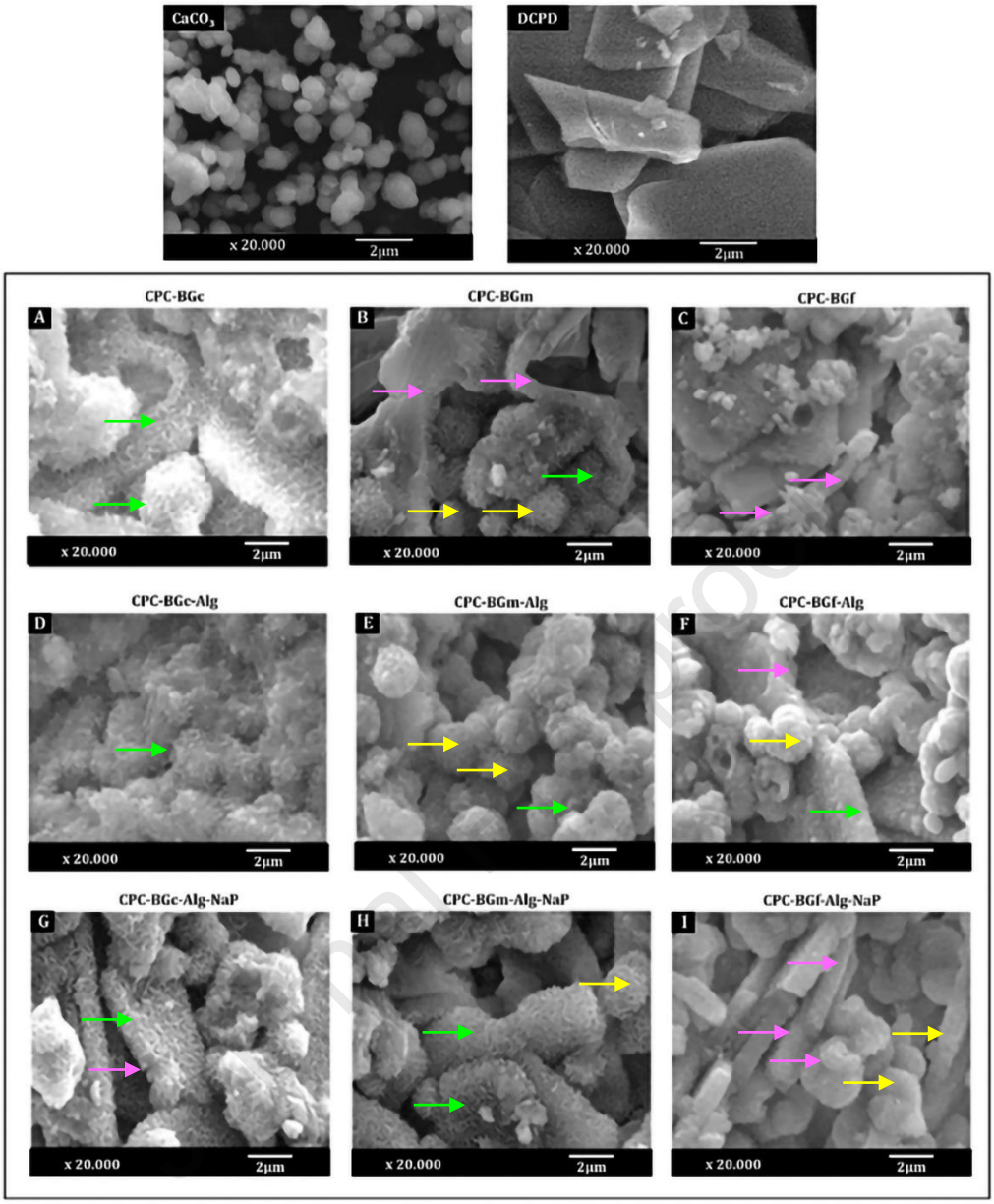

Figure 8. SEM micrographs at 2µm of CPC-BGc (A), CPC-BGm (B), CPC-BGf (C), CPC-BGc-Alg (D), CPC-BGm-Alg (E), CPC-BGf-Alg (F), CPC-BGc-Alg-NaP (G), and CPC-BGm-Alg-NaP (H), and CPC-BGm-Alg-NaP (I). (Yellow arrows: vaterite, pink arrows: bioactive glass, green arrows: apatite).

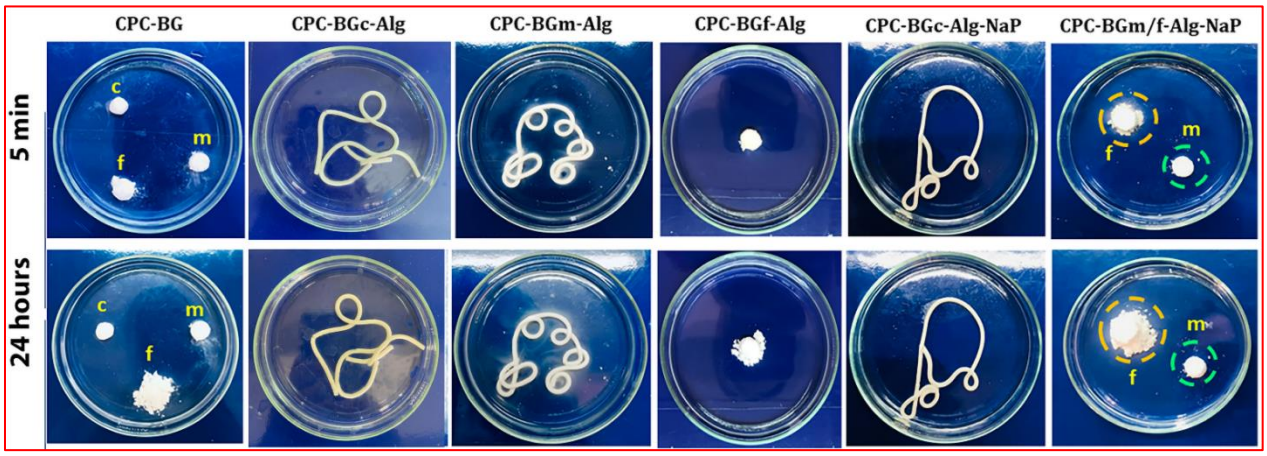

Figure 9. Photos of formulated pastes taken after 5 minutes and 24 hours of immersion in PBS solution (c: coarse, m: medium, and f: fine).

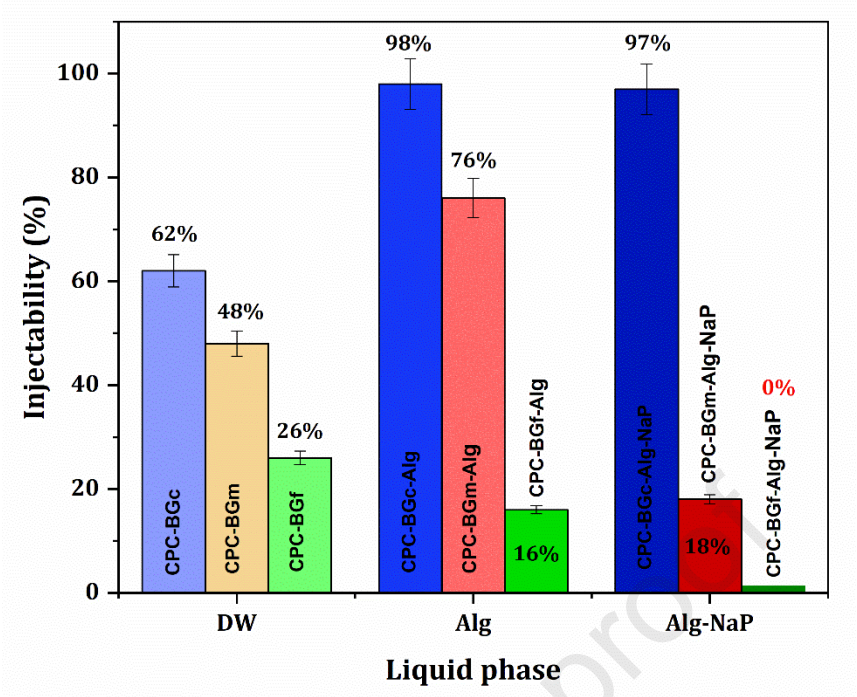

Figure 10. Injectability values of prepared materials regarding the BG particle size and the nature of the liquid phase.

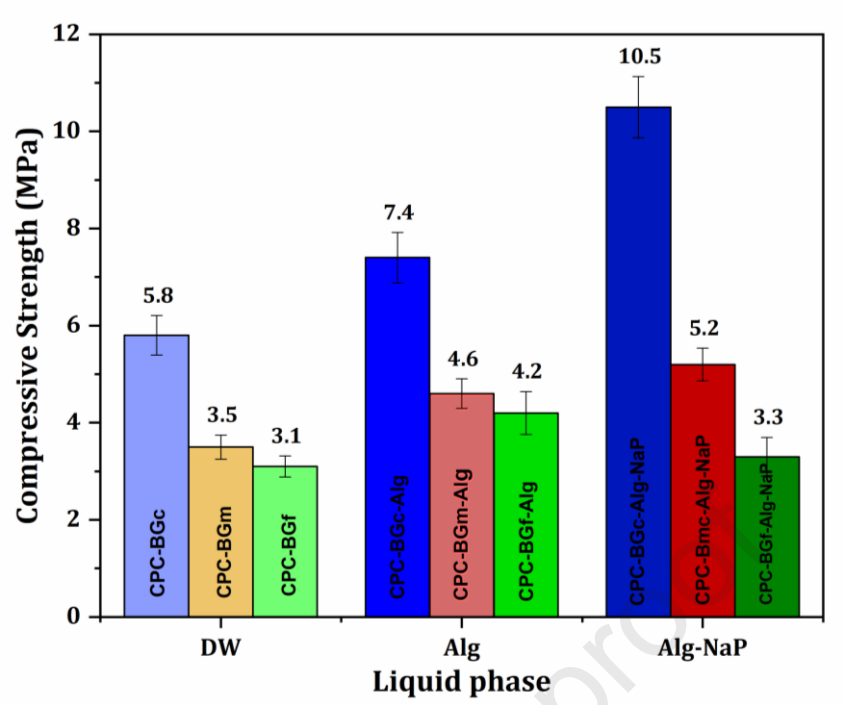

Figure 11. Compressive strength of prepared cement composites, as a function of BG particle size and the liquid phase nature.

Declaration of interests

☒ The authors declare that they have no known competing financial interests or personal relationships that could have appeared to influence the work reported in this paper.

☐The authors declare the following financial interests/personal relationships which may be considered as potential competing interests: